

---


Electronic Theses and Dissertations, 2004-2019

---

2015

## An Improved Biosolid Gasifier Model

Hannah McLean  
*University of Central Florida*

 Part of the [Environmental Engineering Commons](#)  
Find similar works at: <https://stars.library.ucf.edu/etd>  
University of Central Florida Libraries <http://library.ucf.edu>

This Masters Thesis (Open Access) is brought to you for free and open access by STARS. It has been accepted for inclusion in Electronic Theses and Dissertations, 2004-2019 by an authorized administrator of STARS. For more information, please contact [STARS@ucf.edu](mailto:STARS@ucf.edu).

---

### STARS Citation

McLean, Hannah, "An Improved Biosolid Gasifier Model" (2015). *Electronic Theses and Dissertations, 2004-2019*. 1151.  
<https://stars.library.ucf.edu/etd/1151>

AN IMPROVED BIOSOLID GASIFIER MODEL

by

HANNAH MCLEAN, E.I.  
B.S.Env.E., University of Central Florida, 2013

A thesis submitted in partial fulfillment of the requirements  
for the degree of Master of Science  
in the Department of Civil, Environmental, and Construction Engineering  
in the College of Engineering and Computer Science  
at the University of Central Florida  
Orlando, Florida

Spring Term  
2015

Major Professor: C. David Cooper

## ABSTRACT

As populations increase and cities become denser, the production of waste, both sewage sludge and food biomass, increases exponentially while disposal options for these wastes are limited. Landfills have minimal space for biosolids; countries are now banning ocean disposal methods for fear of the negative environmental impacts. Agricultural application of biosolids cannot keep up with the production rates because of the accumulation of heavy metals in the soils. Gasification can convert biosolids into a renewable energy source that can reduce the amount of waste heading to the landfills and reduce our dependence on fossil fuels.

A recently published chemical kinetic computer model for a fluidized-bed sewage sludge gasifier (Champion, Cooper, Mackie, & Cairney, 2014) was improved in this work based on limited experimental results obtained from a bubbling fluidized-bed sewage sludge gasifier at the MaxWest facility in Sanford, Florida and published information from the technical literature. The gasifier processed sewage sludge from the communities surrounding Sanford and was operated at various air equivalence ratios and biosolid feed rates. The temperature profile inside of the gasifier was recorded over the span of four months, and an average profile was used in the base case scenario.

The improved model gave reasonable predictions of the axial bed temperature profile, syngas composition, heating value of the syngas, gas flow rate, and carbon conversion. The model was validated by comparing the simulation temperature profile data with the measured temperature profile data. An overall heat loss coefficient was calculated for the gasification unit to provide a more accurate energy balance. Once the model was equipped with a heat loss

coefficient, the output syngas temperature closely matched the operational data from the MaxWest facility.

The model was exercised at a constant equivalence ratio at varying temperatures, and again using a constant temperature with varying equivalence ratios. The resulting syngas compositions from these exercises were compared to various literature sources. It was decided that some of the reactions kinetics needed to be adjusted so that the change in syngas concentration versus change in bed temperature would more closely match the literature. The reaction kinetics for the Water-Gas Shift and Boudouard reactions were modified back to their original values previously obtained from the literature.

# TABLE OF CONTENTS

|  |     |
|--|-----|
| LIST OF FIGURES .....  | vii |
| LIST OF TABLES .....   | x   |
| LIST OF ABBREVIATIONS/ACRONYMS .....                         | xi  |
| 1. INTRODUCTION .....  | 1   |
| 1.1 Problem Statement .....                                  | 1   |
| 1.2 Project Objectives .....                                 | 1   |
| 1.3 Project Importance .....                                 | 2   |
| 2. LITERATURE REVIEW .....                                   | 3   |
| 2.1 Overview of Biosolids Gasification .....                 | 3   |
| 2.2 Gasification Modeling .....                              | 7   |
| 2.3 Determining Heat Loss .....                              | 13  |
| 2.4 Effect of Bed Temperature on the Quality of Syngas ..... | 19  |
| 2.5 Effect of Equivalence Ratio on Syngas Quality .....      | 23  |
| 2.6 Use of Temperature as a Fitting Parameter .....          | 25  |
| 3. MAXWEST BIOSOLID GASIFICATION PROCESS .....               | 27  |
| 3.1 Overview of Operations .....                             | 27  |

|         |  |    |
|---------|--|----|
| 3.2     | Data Collection Process .....  | 33 |
| 4.      | DETERMINATION OF HEAT LOSS COEFFICIENT .....                                 | 41 |
| 4.1     | Temperature Profile Comparison.....  | 41 |
| 4.2     | Heat Loss Calculations and Determination of Heat Loss through Freeboard..... | 42 |
| 5.      | SENSITIVITY ANALYSIS .....   | 48 |
| 5.1     | Changing Reaction Kinetics.....  | 48 |
| 5.1.1   | Water-Gas Shift Reaction .....   | 49 |
| 5.1.2   | Boudouard Reaction.....  | 50 |
| 5.2     | Base Design Case Comparison .....  | 59 |
| 5.3     | Delta Cases.....   | 61 |
| 5.3.1   | Varying Equivalence Ratio at Constant Temperature .....                      | 61 |
| 5.3.2   | Varying Temperature at Constant Equivalence Ratio .....                      | 65 |
| 5.3.3   | Varying Biosolid Composition .....   | 67 |
| 5.3.3.1 | Carbon .....   | 68 |
| 5.3.3.2 | Hydrogen .....   | 69 |
| 5.3.3.3 | Nitrogen.....  | 70 |
| 6.      | RESULTS AND MODEL IMPROVEMENTS.....  | 71 |

|     |  |    |
|-----|--|----|
| 6.1 | Final Model .....  | 71 |
| 7.  | CONCLUSIONS AND RECOMMENDATIONS .....                          | 77 |
| 7.1 | Utility of the Model.....                                      | 77 |
| 7.2 | Recommendations for Future Research .....                      | 78 |
|     | APPENDIX: SUGGESTIONS FOR RUNNING THE GASIFICATION MODEL ..... | 79 |
|     | REFERENCES .....   | 81 |

## LIST OF FIGURES

|  |    |
|--|----|
| Figure 2-1. Overall Process in a Gasifier (Adapted from Gómez-Barea et al., 2010).....   | 7  |
| Figure 2-2. Overview of the Gasification Model (Adapted from Champion et al., 2014) .....  | 9  |
| Figure 2-3. Sketch of a Single Control Volume used for Heat Transfer Analysis (Adapted from Sharma, 2008).....   | 14 |
| Figure 2-4. Effect of Temperature on Parameters and Processes during Gasification (Adapted from Gómez-Barea et al., 2013) .....                                      | 21 |
| Figure 2-5. Comparison between a Single-Stage FBG and a Three-Stage FBG System (FLETGAS) for Sewage Sludge Gasification (Adapted from Gómez-Barea et al., 2013)..... | 23 |
| Figure 3-1. MW2000 Gasification Unit (Adapted from MaxWest Environmental Systems, Inc., 2012) .....  | 29 |
| Figure 3-2. MaxWest Process Equipment .....  | 32 |
| Figure 3-3. Gasifier Steady-State Temperatures.....  | 37 |
| Figure 3-4. Temperature Profile in Gasifier .....  | 38 |
| Figure 4-1. Temperature Profile Comparison using Heat Loss as a Percentage (model M1) .....  | 44 |
| Figure 4-2. Temperature Profile Comparison using Heat Loss Coefficient (model M2).....   | 45 |
| Figure 4-3. Temperature Profile Comparison with Heat Loss Coefficient = 4.0 J/m-s-K (model M3).....  | 47 |



|  |    |
|--|----|
| Figure 5-1. CO Concentration vs Varying Temperature at ER=0.30 .....   | 52 |
| Figure 5-2. CO <sub>2</sub> Concentration vs Varying Temperature at ER=0.30 .....  | 53 |
| Figure 5-3. H <sub>2</sub> Concentration vs Varying Temperature at ER=0.30 .....   | 53 |
| Figure 5-4. Comparison of Model (M1) Predictions (CO) with Literature .....  | 55 |
| Figure 5-5. Comparison of Model (M4) Predictions (CO) with Literature .....  | 55 |
| Figure 5-6. Comparison of Model (M1) Predictions (CO <sub>2</sub> ) with Literature.....   | 56 |
| Figure 5-7. Comparison of Model (M4) Predictions (CO <sub>2</sub> ) with Literature.....   | 56 |
| Figure 5-8. Comparison of Model (M1) Predictions (H <sub>2</sub> ) with Literature .....   | 57 |
| Figure 5-9. Comparison of Model (M4) Predictions (H <sub>2</sub> ) with Literature .....   | 57 |
| Figure 5-10. Comparison of Model (M1) Predictions (CH <sub>4</sub> ) with Literature.....  | 58 |
| Figure 5-11. Comparison of Model (M4) Predictions (CH <sub>4</sub> ) with Literature.....  | 58 |
| Figure 5-12. Syngas Composition with New Pre-Exponential Factors in Boudouard and Water-Gas Shift Reactions (at constant ER=0.21)..... | 59 |
| Figure 5-13. Syngas Composition vs Varying ER, T=1200 °F .....   | 63 |
| Figure 5-14. Syngas Composition vs Varying ER, T=1300 °F .....   | 63 |
| Figure 5-15. Syngas Composition vs Varying ER, T=1400 °F .....   | 64 |
| Figure 5-16. Higher Heating Value vs Varying ER, 1300°F .....  | 64 |

|   |    |
|---|----|
| Figure 5-17. Syngas Composition vs Varying Temperature, ER=0.21 .....                     | 66 |
| Figure 5-18. Syngas Composition vs Varying Temperature, ER=0.30 .....                     | 66 |
| Figure 5-19. Syngas Composition vs Varying Temperature, ER=0.40 .....                     | 67 |
| Figure 5-20. Syngas Composition vs Varying Carbon Content in Feed, ER=0.21, T=1300°F .... | 68 |
| Figure 5-21. Syngas Composition vs Varying Hydrogen Content in Feed, ER=0.21, T=1300°F    | 69 |
| Figure 5-22. Syngas Composition vs Varying Nitrogen Content in Feed, ER=0.21, T=1300°F .  | 70 |
| Figure 6-1. Gasifier Model GUI-Inputs Screen .....  | 73 |
| Figure 6-2. Gasifier Model GUI-Outputs Screen .....                                       | 74 |
| Figure 6-3. Base Case Results .....   | 74 |

## LIST OF TABLES

|  |    |
|--|----|
| Table 2-1. Ultimate Analyses for Biosolids.....  | 4  |
| Table 2-2. Proximate Analyses for Biosolids .....  | 4  |
| Table 2-3. Elemental Analysis of Ash .....   | 5  |
| Table 2-4. Modified Kinetic Constants of Primary Reactions Utilized in Model .....       | 12 |
| Table 2-5. Reactions Occurring in Oxidation Zone.....                                    | 13 |
| Table 2-6. Reactions Occurring in Reduction Zone .....                                   | 14 |
| Table 2-7. Molar Heat Capacity Constants.....  | 16 |
| Table 3-1. Base Case Operation Data* .....   | 34 |
| Table 3-2. Base Case Gasifier Temperature Profile* .....                                 | 35 |
| Table 5-1. Model (M4) Output Compared to Experimental Literature .....                   | 60 |
| Table 5-2. Key Reactions Assumed to Occur in a Gasifier .....                            | 61 |
| Table 5-3. Key Tar Cracking and Oxidation Reactions Assumed to Occur in a Gasifier ..... | 62 |

## LIST OF ABBREVIATIONS/ACRONYMS

|                               |                                   |
|-------------------------------|-----------------------------------|
| °C                            | degrees Celcius                   |
| °F                            | degrees Fahrenheit                |
| A                             | Area                              |
| APC                           | Air pollution control             |
| BFB                           | Bubbling fluidized bed            |
| Btu                           | British thermal unit              |
| C                             | Solid char or carbon              |
| C <sub>6</sub> H <sub>6</sub> | Benzene                           |
| CFB                           | Circulating fluidized bed         |
| CH <sub>4</sub>               | Methane                           |
| Cl                            | Chlorine                          |
| C <sub>m</sub> H <sub>n</sub> | Representation of tar species     |
| CO                            | Carbon monoxide                   |
| CO <sub>2</sub>               | Carbon dioxide                    |
| C <sub>p</sub>                | Heat capacity (molar or specific) |
| CSTR                          | Continuously Stirred Tank Reactor |
| DD                            | Drying and Devolatilization       |
| e                             | Exponential                       |
| ER                            | Equivalence ratio                 |

|         |                             |
|---------|-----------------------------|
| f       | Molar fraction              |
| FBG     | Fluidized-bed gasifier      |
| ft      | Foot                        |
| fuel-C  | Biomass carbon              |
| fuel-Cl | Biomass chlorine            |
| fuel-H  | Biomass hydrogen            |
| fuel-N  | Biomass nitrogen            |
| fuel-O  | Biomass oxygen              |
| fuel-S  | Biomass sulfur              |
| gmol    | Gram mole                   |
| GUI     | Graphical User Interface    |
| H       | Enthalpy                    |
| $H_g$   | Enthalpy of gaseous species |
| $H_s$   | Enthalpy of solid species   |
| $H_2$   | Molecular hydrogen          |
| $H_2O$  | Water vapor                 |
| $H_2S$  | Hydrogen sulfide            |
| HCl     | Hydrogen chloride           |
| HHV     | Higher heating value        |
| i       | Summation index             |
| j       | Summation index             |

|                   |                                    |
|-------------------|------------------------------------|
| J                 | Joules                             |
| K                 | Kelvin                             |
| k                 | Reaction rate pre-exponential term |
| kg                | Kilogram                           |
| kJ                | Kilojoules                         |
| lb                | Pound-mass                         |
| LHV               | Lower heating value                |
| m                 | Meter                              |
| N <sub>2</sub>    | Molecular nitrogen                 |
| NH <sub>3</sub>   | Ammonia                            |
| NO <sub>x</sub>   | Nitrous Oxide                      |
| OX                | Oxidation                          |
| P                 | Pressure                           |
| q <sub>L</sub>    | Heat loss term                     |
| Q                 | Volumetric flow rate               |
| Q <sub>loss</sub> | Net heat loss                      |
| R                 | Ideal gas law constant             |
| r                 | Reaction rate                      |
| RED               | Reduction                          |
| s                 | Second                             |
| SO <sub>2</sub>   | Sulfur dioxide                     |

|              |                            |
|--------------|----------------------------|
| T            | Temperature                |
| t            | Time                       |
| U            | Heat loss coefficient      |
| V            | Volume                     |
| $\Delta H_r$ | Heat of reaction           |
| $\Sigma$     | Sigma notation (summation) |

# 1. INTRODUCTION

## 1.1 Problem Statement

The thermochemical gasifier model developed by Champion et al. (2014) was based on detailed chemical reaction models, engineering calculations, and kinetic data reported in the scientific literature. Actual operational data from the MaxWest commercial-scale sewage sludge gasification facility in Sanford, Florida were also used. These operational data were used to adjust the gasifier model so that temperature predictions more closely matched the facility's steady-state temperature profile. The predicted syngas composition and flow rate are key results of the gasification model and are important inputs for the modeling of syngas combustion in their thermal oxidizer. The modeling of both gasification of sewage sludge and the combustion of the syngas will provide the information needed for the proper operation of the downstream air pollution control (APC) equipment at the facility.

## 1.2 Project Objectives

The main objective of this research project was to validate and improve the accuracy of the gasifier computer model developed by Champion et al. (2014) for MaxWest Environmental Systems, Inc. Operational data were collected from the MaxWest facility along with recent literature and were used to validate and improve the kinetic model. This validation was done through the comparison of the modeled temperature profile and of the operational temperature data throughout the gasifier unit.



### 1.3 Project Importance

The improved computer model resulting from this project will aid in the future design of gasifiers as well as APC equipment used in the gasification/oxidation processes. Through the increased understanding of biosolid gasification, this process can be made more efficient and can become a more viable option as a renewable energy source. This kinetic model adjusted to the MaxWest facility provides the client with an improved tool that will be used to make their operations more efficient and profitable.

The characteristics of syngas produced by gasification can be very different depending on the various operating conditions (bed temperature, pressure, air-to-fuel ratio, moisture content, and chemical make-up of feed material) under which the reactions take place. The effects of each parameter should be investigated and model results should be validated for producing high-quality syngas.

## 2. LITERATURE REVIEW

### 2.1 Overview of Biosolids Gasification

Biosolids are the solids produced by wastewater treatment plants and consist of biomass, silt, sand, bits of plants, algae, bacteria, and chemical precipitates. The rate of biosolids production is rising while the disposal methods are becoming increasingly restricted. Agriculture application of biosolids as a soil enhancer is one method of disposal, but is limited because of the accumulation of heavy metals and phosphates in the soil (Adegoye et al., 2004). Landfill disposal is another method often employed by wastewater treatment facilities, but, as populations increase, so does the production of solid waste. Landfill sites are filling up with all forms of waste and do not have much room for biosolids.

Biosolids coming out of secondary or tertiary treatment contain about 98% water content and require extensive dewatering to about 25% solids before they can be dried and used for gasification. The dryer system can remove water to obtain a dry material with about 90% solids content (Wang, Rudolph, & Zhu, 2008). Specific ratios of the major elements in biosolids range from location to location based on local diets, industrial flows, and other factors. Average values for the proximate and ultimate analyses of biosolids and ash are shown in Tables 2-1 and 2-2 (Roy, Dutta, Corscadden, Havard, & Dickie, 2011; Manyà, Aznar, Sánchez, Arauzo, & Murilla, 2006; Houdková, Boran, Ucekaj, Elsasser, & Stehlik, 2008; Werther & Ogada, 2009; Cartmell et al., 2006; University of Hawaii, 2002; Yuan et al., 2011) and Table 2-3 (University of Hawaii, 2002). Ultimate analysis is the determination of the amount of carbon, hydrogen, nitrogen, sulfur, oxygen, chlorine, and ash in a species and the proximate analysis is the determination of the amount of moisture, volatile matter, fixed carbon, and ash in the species (ASTM D 3176 and 121 respectively).

**Table 2-1. Ultimate Analyses for Biosolids**

| Species  | Average |
|----------|---------|
| Carbon   | 39.6%   |
| Hydrogen | 5.44%   |
| Nitrogen | 4.94%   |
| Sulfur   | 1.15%   |
| Oxygen   | 25.2%   |

Source: Roy et al., 2011; Manyà et al., 2006; Houdková et al., 2008; Werther & Ogada, 2009; Cartmell et al., 2006; University of Hawaii, 2002; Yuan et al., 2011

**Table 2-2. Proximate Analyses for Biosolids**

| Species  | Average |
|----------|---------|
| Volatile | 62.7%   |
| Moisture | 51.7%   |
| Fixed C  | 7.60%   |
| Ash      | 31.0%   |

Source: Roy et al., 2011; Manyà et al., 2006; Houdková et al., 2008; Werther & Ogada, 2009; Cartmell et al., 2006; University of Hawaii, 2002; Yuan et al., 2011

**Table 2-3. Elemental Analysis of Ash**

| Species                        | Average |
|--------------------------------|---------|
| SiO <sub>2</sub>               | 30.35%  |
| Al <sub>2</sub> O <sub>3</sub> | 17.8%   |
| TiO <sub>2</sub>               | 2.1%    |
| Fe <sub>2</sub> O <sub>3</sub> | 8.21%   |
| CaO                            | 11.62%  |
| MgO                            | 3.4%    |
| Na <sub>2</sub> O              | 1.1%    |
| K <sub>2</sub> O               | 1.16%   |
| P <sub>2</sub> O <sub>5</sub>  | 20.4%   |
| SO <sub>3</sub>                | 2.4%    |
| Cl                             | .06%    |
| CO <sub>2</sub>                | .45%    |

Source: University of Hawaii, 2002

Until recently, combustion has been the primary method of generating heat from burning renewable and nonrenewable fuels such as wood, coal and natural gas. Coal gasification, a fairly old process, has been used to extract energy from coal as a more environmentally friendly alternative to combustion. Gasification of wood, as well as other wastes and sewage sludge is now being used to generate energy. Even though gasification of these waste products produces less energy than fossil fuels, the carbon dioxide released does not have the potential to further enhance the greenhouse effect, since the sources are not of ancient origin (Adegoroye et al., 2004).

Gasification is the thermo-chemical conversion of solid carbonaceous materials in an oxygen-limited environment to produce combustible fuel gases. Gasification is not combustion

because combustion allows for the complete or nearly complete oxidation of all of the organic compounds in the fuel. Similarly gasification is not pyrolysis because the reactions in a gasifier do not take place in an oxygen-absent environment. In gasification, the amount of air used is much less than the stoichiometric amount needed for complete combustion but allows for partial oxidation of the organic fuel. These oxidation reactions generate the heat needed for the subsequent reduction (gasification) reactions.

Biosolids gasification has many advantages over other means of disposal: destruction of pathogenic bacteria, lower-cost air emissions control, large reduction of waste volume, and energy production. The efficiency of the gasification process is theoretically higher than that of incineration because the produced syngas can be used directly to generate power (Roy et al., 2011). One of the main drawbacks of biosolid gasification is the high tar and dust content of the syngas. Tar is undesirable because of various phenomena involving condensation, formation of tar aerosols, and polymerization that forms more complex structures (Roy et al., 2011). The high dust content of the syngas can cause blockage of downstream equipment and ducts. Both tars and dust can cause serious problems in downstream engines and turbines.

In biomass gasification, a highly combustible mixture of gases is produced and is referred to as syngas or product gas. The syngas primarily consists of carbon monoxide (CO), hydrogen (H<sub>2</sub>), methane (CH<sub>4</sub>), nitrogen (N<sub>2</sub>), water vapor (H<sub>2</sub>O), carbon dioxide (CO<sub>2</sub>), hydrogen sulfide (H<sub>2</sub>S), ammonia (NH<sub>3</sub>), and traces of higher hydrocarbons and other gases such as SO<sub>2</sub> and HCl (Miao et al., 2014; Liu & Gibbs, 2002). The process of gasification can be summarized in the following steps: drying of the fuel, pyrolysis, oxidation and reduction reactions, and gas-phase reactions (see Figure 2-1). These reactions are carried out at high temperatures ranging from

1100 °F to 1600 °F; however at temperatures above 1360 °F, unwanted ash agglomeration can occur (MaxWest Environmental Systems, Inc., 2013).

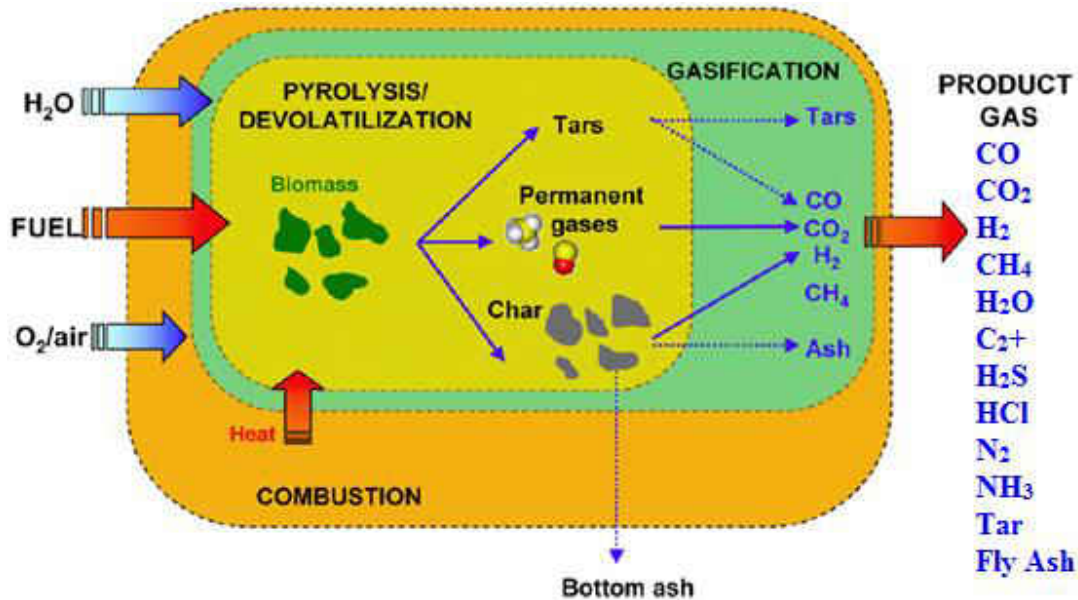


Figure 2-1. Overall Process in a Gasifier (Adapted from Gómez-Barea et al., 2010)

## 2.2 Gasification Modeling

There are two main approaches to modeling the gasification process: thermodynamic equilibrium and chemical kinetics. In thermodynamic equilibrium, the products and reactants are in dynamic equilibrium and the concentrations of gases do not change. These concentration calculations are dependent upon equilibrium factors and an assumed temperature. This assumption can result in an overestimation of the concentrations of H<sub>2</sub> and CO in the syngas, and an underestimation of CO<sub>2</sub>, tars, and ash-bound char (Puig-Arnabat, Bruno, & Coronas, 2010). However it is not widely expected that the gasification reactions will proceed to completion nor that equilibrium will be achieved in the gasifier (Basu & Kaushal, 2010). This is why a more realistic modeling process should be based on chemical kinetics. Since the temperature in a

gasifier may change with height, the syngas composition may also change. With a chemical kinetic model it is possible to predict the syngas composition at various heights in the gasifier.

One of the kinetic models reviewed defined the gasification process as essentially two steps: the drying and pyrolysis of the biomass (assumed to occur simultaneously), followed by the gasification of the volatile gases produced in the first step (Petersen & Werther, 2005). In the drying and pyrolysis zone, it was assumed that water is vaporized and that the biomass is devolatilized into gases, char, and tar. The second zone included the oxidation and reduction reactions affecting the gases, char, and tar produced in the drying and pyrolysis zone.

Another approach is to model the process as three steps: (1) drying and pyrolysis, (2) partial oxidation of the biosolids, and (3) gasification (reduction) reactions. Champion et al. (2014) developed a one-dimensional, nonisothermal thermochemical model to predict the syngas rate and composition from a commercial-scale bubbling fluidized-bed sewage sludge gasifier using a three step approach. Detailed kinetic and operational data were obtained from published literature and used to develop and calibrate a model. The model uses input data including biosolids proximate and ultimate analysis, and operating and design parameters of the bubbling-fluidized bed gasifier to predict the final syngas rate, composition, temperature, carbon conversion, and energy content. The model requires the user to input the sludge analysis data and feed rate, the air and recycled flue gas rates, and heat loss (as a percentage). The user interface also provides default values for all inputs and verifies that the user input data are valid.

This specific model describes the behavior of an upflow fluidized-bed gasifier in which biosolids and air enter at the bottom of the gasifier and the syngas and ash exit at the top of the gasifier. The composition of the gases change with location in the gasifier bed which was

modeled as a plug flow reactor, and approximated by 10 continuously stirred tank reactors (CSTRs) in series (see Figure 2-2).

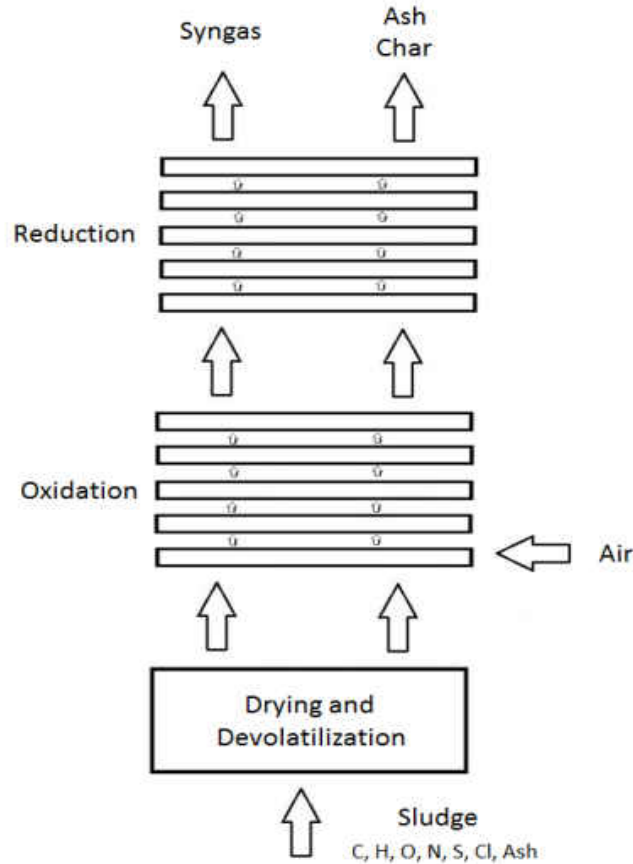


**Figure 2-2. Overview of the Gasification Model (Adapted from Champion et al., 2014)**

The drying and devolatilization (DD) reactions were assumed to occur in two major steps: (1) drying, ash separation, and initial gas formation and (2) dry gas, solid char, and tar formation (Champion et al., 2014). The first step (drying, ash separation, and initial gas formation) produces moisture, mineral ash, organic ash and certain gases such as  $\text{NH}_3$ ,  $\text{H}_2\text{S}$ , and  $\text{HCl}$ . The fuel-bound nitrogen forms  $\text{NH}_3$  and  $\text{N}_2$ ; the fuel-bound sulfur forms  $\text{H}_2\text{S}$  due to the reducing environment in the gasifier; and the fuel-bound chlorine forms  $\text{HCl}$  primarily (Petersen



& Werther, 2005). The remaining biomass (C, H, and O) is called “volatiles” and forms products in the second step (dry-gas, solid char, and tar formation). The dry-gas constituents produced were modeled as CO, CO<sub>2</sub>, CH<sub>4</sub>, and H<sub>2</sub> (Champion et al., 2014). The model solves the DD zone mass balances algebraically. The subsequent values are then used as inputs into the first CSTR in the oxidation zone.

The zones following the drying and devolatilization zone are the oxidation and reduction zones. The air enters the gasifier in the oxidation zone so there is still oxygen present to oxidize the char, CO, CH<sub>4</sub>, H<sub>2</sub> and tars from the DD zone. In the reduction zone, a number of important reactions produce combustible components (H<sub>2</sub>, CO and CO<sub>2</sub>) from the products of the oxidation zone. Each zone was modeled using five CSTRs; the kinetic equations used in these zones are given in Tables 2-4 and 2-5. The reaction kinetics were obtained from the literature and calibrated using a “curve-fitting” procedure (Champion et al., 2014). It was necessary to adjust some of the kinetics constants in the model because the model did not predict well compared to three published experimental studies using laboratory-scale sewage sludge bubbling fluidized-bed gasifiers (de Andrés, Narros, & Rodríguez, 2011; Manyà et al., 2006; Kang, Dong, Kim, Lee, & Hwang, 2011).

Within each CSTR, 18 simultaneous equations account for the mass balances of the 14 gaseous species (O<sub>2</sub>, CO, CO<sub>2</sub>, H<sub>2</sub>, CH<sub>4</sub>, H<sub>2</sub>O, C<sub>6</sub>H<sub>6</sub>, C<sub>6</sub>H<sub>6</sub>O, C<sub>10</sub>H<sub>8</sub>, NH<sub>3</sub>, HCl, H<sub>2</sub>S, N<sub>2</sub>, and Ar), two solid species (char and mineral ash), a total molar balance for the gas stream, and an energy balance for the CSTR. These nonlinear equations are solved simultaneously using a variant of the Newton-Raphson method. This method, named after Isaac Newton and Joseph Raphson, solves for the roots of simultaneous non-linear equations. The specific choice of updating terms is based on an approximation of the function,  $f(x)$ , with a truncated Taylor Series expansion. This

process repeats for each of the 10 CSTRs (Champion et al., 2014). The outputs from the final CSTR are the outputs from the gasifier and include final syngas composition and flow rate, final ash composition and mass, and final syngas temperature. This information is presented on an output screen and in an Excel spreadsheet.

Champion et al. (2014) made large changes to the kinetic constants for the oxidation reactions of tars and methane (see Table 2-4). Champion et al. (2014) justified these changes because the literature from which they were derived determined the kinetics in high temperature experiments using different types of fuel and different types of reactors. These experimental conditions do not translate directly to the oxygen-starved environment in a gasifier (Champion et al., 2014). These changes made to the chemical kinetic constants produced reasonably good performance when the model predictions of the five principal gaseous species (CO, H<sub>2</sub>, CH<sub>4</sub>, CO<sub>2</sub>, and C<sub>6</sub>H<sub>6</sub>) were compared against the experimental data from the literature.

**Table 2-4. Modified Kinetic Constants of Primary Reactions Utilized in Model**

| #  | Reaction   | Lit. $k$              | Model $k$             |
|----|--|-----------------------|-----------------------|
| 1  | $\alpha C (s) + O_2 \rightarrow 2(\alpha-1) CO + (2-\alpha) CO_2$            | 29.8                  | $2.98 \cdot 10^{-1}$  |
| 2  | $CO + 0.5 O_2 \rightarrow CO_2$  | $1.78 \cdot 10^{10}$  | $8.90 \cdot 10^9$     |
| 3  | $CH_4 + 0.5 O_2 \rightarrow CO + 2 H_2$                                      | $1.58 \cdot 10^{12}$  | $7.90 \cdot 10^{10}$  |
| 4  | $H_2 + 0.5 O_2 \rightarrow H_2O$   | $1.08 \cdot 10^7$     | $5.40 \cdot 10^7$     |
| 5  | $C (s) + 1.2 H_2O \rightarrow 0.8 CO + 0.2 CO_2 + 1.2 H_2$                   | $2.39 \cdot 10^2$     | 2.39                  |
| 6  | $H_2O + CO \leftrightarrow H_2 + CO_2$                                       | $2.78 \cdot 10^{-1}$  | $2.78 \cdot 10^{-2}$  |
| 7  | $C (s) + CO_2 \rightarrow 2 CO$  | $3.18 \cdot 10^7$     | $3.18 \cdot 10^5$     |
| 8  | $H_2O + CH_4 \leftrightarrow CO + 3 H_2$                                     | $4.92 \cdot 10^{-11}$ | $4.92 \cdot 10^{-11}$ |
| T1 | $C_6H_6O \rightarrow CO + 0.4 C_{10}H_8 + 0.15 C_6H_6 + 0.1 CH_4 + 0.75 H_2$ | $10^7$                | $10^7$                |
| T2 | $C_6H_6O + 3 H_2O \rightarrow 4 CO + 2 CH_4 + 2 H_2$                         | $10^7$                | $10^7$                |
| T3 | $C_{10}H_8 \rightarrow 7.38 C (s) + 0.275 C_6H_6 + 0.97 CH_4 + 1.235 H_2$    | $1.70 \cdot 10^{14}$  | $1.70 \cdot 10^{14}$  |
| T4 | $C_6H_6 + 2 H_2O \rightarrow 1.5 C (s) + 2.5 CH_4 + 2 CO$                    | $2.00 \cdot 10^{16}$  | $1.00 \cdot 10^{21}$  |
| T5 | $C_6H_6O + 4 O_2 \rightarrow 3 H_2O + 6 CO$                                  | 655                   | $6.55 \cdot 10^{-1}$  |
| T6 | $C_6H_6 + 4.5 O_2 \rightarrow 3 H_2O + 6 CO$                                 | $2.40 \cdot 10^{11}$  | $1.20 \cdot 10^7$     |
| T7 | $C_{10}H_8 + 7 O_2 \rightarrow 4 H_2O + 10 CO$                               | 665                   | $6.65 \cdot 10^{-1}$  |

Source: Champion et al., 2014

The model validation consisted of using the remaining data sets (not used for model calibration) from the experimental studies and statistical analysis to compare the predicted gaseous compositions with literature values (Champion et al., 2014; de Andrés et al., 2011; Manyà et al., 2006; Kang et al., 2011). The Ansari-Bradley statistical method was chosen

because it does not rely on the data sets to have normal distributions (Mendenhall and Sincich, 2007). With a 95% confidence interval, the authors were unable to disprove the null hypothesis that the literature and model data sets had the same median, shape, and distribution (Champion et al., 2014). Predicted tar content was the only component to have a considerable number of values outside of the confidence interval.

### 2.3 Determining Heat Loss

In fluidized-bed gasifiers, the sand in the bottom section of the gasifier (the fluidizing material) keeps the temperature profile in the gasifier bed relatively constant. Tables 2-5 and 2-6 express the reactions taking place in the oxidation and reduction zones of the gasifier as well as their standard heats of reaction.

**Table 2-5. Reactions Occurring in Oxidation Zone**

| <b>Reaction Name</b> | <b>Reaction</b>                                    | <b><math>\Delta H_r, 298K</math> (kJ/mol)</b> |
|----------------------|--|---|
| Char Oxidation       | $C(s) + \frac{1}{2} O_2(g) \rightarrow CO(g)$      | -110.5  |
| Char Oxidation       | $C(s) + O_2(g) \rightarrow CO_2(g)$                | -393.5  |
| Char Oxidation       | $CO(g) + \frac{1}{2} O_2(g) \rightarrow CO_2(g)$   | -283.0  |
| Oxidation            | $H_2(g) + \frac{1}{2} O_2(g) \rightarrow H_2O(g)$  | -241.8  |
| Oxidation            | $CH_4(g) + 2O_2(g) \rightarrow CO_2(g) + 2H_2O(g)$ | -802.3  |

**Table 2-6. Reactions Occurring in Reduction Zone**

| Reaction Name   | Reaction  | $\Delta H_{r, 298K}$ (kJ/mol) |
|-----------------|---|-------------------------------|
| Methanation     | $C(s) + 2H_2(g) \rightarrow CH_4(g)$            | -74.87                        |
| Water-Gas Shift | $H_2O(g) + CO(g) \rightarrow H_2(g) + CO_2(g)$  | -41.17                        |
| Boudouard       | $C(s) + CO_2(g) \rightarrow 2CO(g)$             | 172.5                         |
| Water-Gas       | $C(s) + H_2O(g) \rightarrow H_2(g) + CO(g)$     | 131.3                         |
| Steam Reforming | $H_2O(g) + CH_4(g) \rightarrow CO(g) + 3H_2(g)$ | 206.2                         |

Heat gain from the exothermic reactions, heat loss from the endothermic reactions, heat loss through the walls to the surroundings, and conduction and radiation heat transfer between adjacent control volumes, should be taken into account when modeling a biomass gasifier (Sharma, 2008).

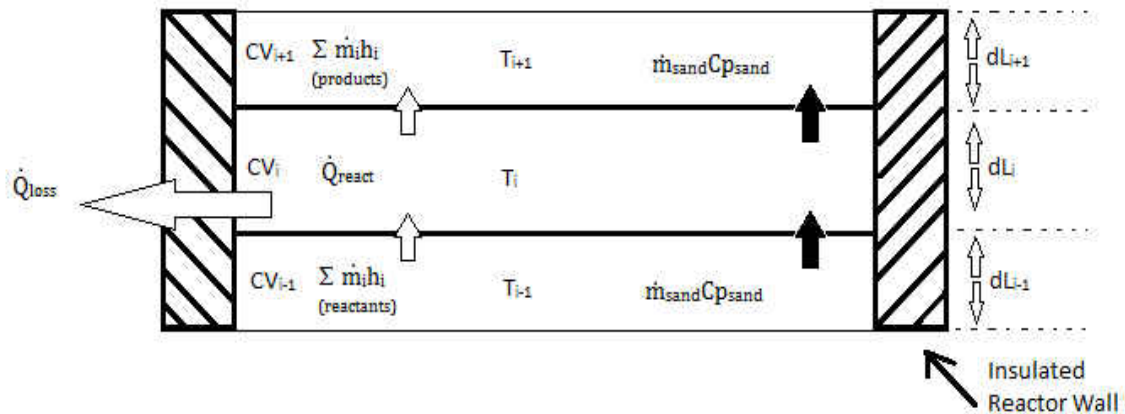


**Figure 2-3. Sketch of a Single Control Volume used for Heat Transfer Analysis (Adapted from Sharma, 2008)**

In the reduction zone there is a mixture of gases and char so an accurate heat loss model would include specific heats for char and for all of the gases in the gas mixture. Sharma (2008) gives the following equations for determining specific heats for the char and gas species:

$$C_{p \text{ char}} = 1.39 + 0.00036T \quad (2-1)$$

$$C_{p \text{ gas-mixture}} = \sum_{\text{gases}} Y_i C_{pi} \quad (2-2)$$

Where:

$C_p$  = specific heat (kJ/kg-K)

$Y_i$  = mole fraction

$T$  = temperature (K)

The change in enthalpy of any gas in the mixture, ignoring the influence of char since it does not contribute significant heat capacity, can be expressed by the following equation:

$$\Delta H_i = \int \dot{n}_i * C_{pi} * dT \quad (2-3)$$

Where:

$\Delta H_i$  = change in enthalpy for specie  $i$  (Btu/hr)

$C_{pi}$  = specific heat of specie  $i$  (Btu/lbmol-°F)

$\dot{n}_i$  = molar flow rate of specie  $i$  ( $\frac{\text{lbmol}}{\text{hr}}$ )

Taking into consideration the molar heat capacities of each gas in the mixture and the difference in temperature, the above equation can be directly integrated between some reference temperature and the final temperature and then summed to achieve the specific enthalpy of the gas mixture:

$$\Delta H_T = \sum \Delta H_i = \sum n_i(\alpha_i * (T_2 - T_1) + \frac{\beta_i}{2} * (T_2^2 - T_1^2) + \frac{\gamma_i}{3} * (T_2^3 - T_1^3)) \quad (2-4)$$

Where:

$\Delta H_T =$  total enthalpy change for the gas mixture ( $\frac{Btu}{hr}$ )

$\alpha_i, \beta_i, \gamma_i =$  molar heat capacity coefficients for specie  $i$

$T_2 =$  temperature leaving zone in gasifier (K)

$T_1 =$  temperature entering zone in gasifier (K)

The prominent gaseous species in the gasifier are given in Table 2-7 along with their corresponding molar heat capacity coefficients for the temperature range 298-1000 K (Santolero, Reynolds, & Theodore, 2000).

**Table 2-7. Molar Heat Capacity Constants**

| Components                               | $\alpha$ | $\beta$  | $\gamma$  |
|--|----------|----------|-----------|
| <b>O<sub>2</sub></b>                     | 6.148    | 3.10E-03 | -9.23E-07 |
| <b>CO</b>                                | 6.42     | 1.67E-03 | -1.96E-07 |
| <b>CO<sub>2</sub></b>                    | 6.214    | 1.04E-02 | -3.55E-06 |
| <b>H<sub>2</sub></b>                     | 6.947    | 2.00E-04 | 4.81E-07  |
| <b>CH<sub>4</sub></b>                    | 3.381    | 1.80E-02 | -4.30E-06 |
| <b>H<sub>2</sub>O</b>                    | 7.256    | 2.30E-03 | 2.83E-07  |
| <b>Tars (C<sub>6</sub>H<sub>6</sub>)</b> | -0.409   | 7.76E-02 | -2.64E-05 |
| <b>NH<sub>3</sub></b>                    | 6.086    | 8.81E-03 | -1.51E-06 |
| <b>HCl</b>                               | 6.732    | 4.33E-04 | 3.70E-07  |
| <b>H<sub>2</sub>S</b>                    | 6.662    | 5.13E-03 | -8.54E-07 |
| <b>N<sub>2</sub></b>                     | 6.184    | 3.10E-03 | -9.23E-07 |
| <b>Ar</b>                                | 6.524    | 1.25E-03 | 1.00E-09  |

Source: Santolero et al., 2000

There are several ways to formulate heat balances for gasification of biomass in a fluidized-bed. An overall heat balance can be applied over the whole reactor: inlets plus generation equal outlets plus losses. Heat balances can be applied over specific regions of the gasifier such as the bed or the secondary air injection zone. Heat balances can be applied over various regions without distinction of phases (gas or solid). Heat balances can also be applied along zones of the reactor including heat and mass transfer between bubble and emulsion phase, gas and solid particles, and heat transfer across external surfaces (Gómez-Barea & Leckner, 2010).

As suggested by Gómez-Barea and Leckner (2010), the heat balance takes into account the changes in enthalpy of the gases in the bubble and emulsion phases due to heat transfer from the solid particles, the bubbles, and exchanges with the surroundings. The overall heat-transfer coefficient for the surroundings is determined by the three mechanisms of heat transfer: bed to wall, conduction through the solid insulation blanket, and free convection caused by the environment. However exact this method can be, it is rarely validated by measurements of instantaneous profiles of gas in the emulsion and bubble phase so this method has not been proven to be much better than models with an overall heat balance for the whole reactor using Equation 2-5 (Yan, Heidenreich, & Zhang, 1999).



$$\Delta H_T = h_e - h_i = \sum h_{rxn} + q_L + \dot{m}_{sand} * C_{p\ sand} * (T_2 - T_1) \quad (2-5)$$

Where:

$$h_e = \text{enthalpy of gases exiting bed } \left(\frac{Btu}{hr}\right)$$

$$h_{rxn} = \text{heats of reaction } \left(\frac{Btu}{hr}\right)$$

$$q_L = \text{heat loss from fluidized bed to surroundings } \left(\frac{Btu}{hr}\right)$$

$$h_i = \text{enthalpy of gases entering bed } \left(\frac{Btu}{hr}\right)$$

$$\dot{m}_{sand} = \text{mass flux of sand } \left(\frac{lb}{hr}\right)$$

$$C_{p\ sand} = \text{molar heat capacity of sand } \left(\frac{Btu}{lbmol - ^\circ F}\right)$$

$$T_2 = \text{temperature leaving zone in gasifier } (^\circ F)$$

$$T_1 = \text{temperature entering zone in gasifier } (^\circ F)$$

$$\Delta H_T = \text{total change in enthalpy of gases } \left(\frac{Btu}{hr}\right)$$

In the above equation, the right hand side refers to the heat entering the fluidized bed carried by the gaseous stream and by the fluidizing agent, sand. The left hand side of the equation refers to the total energy leaving the bed carried by the gaseous streams, heat generated by the chemical reactions, and accounts for heat loss from the fluidized bed to the surroundings (including the environment and freeboard section of the gasifier). The value of the heat loss factor is a function of the fluidized bed and ambient temperatures, insulation of the reactor, and reactor dimensions (Yan et al., 1999). Thus this heat balance is not overly complicated and accounts for the heat entering the system and the heat leaving the system as well as heat loss to the environment. Using these equations and coefficients provided in the literature, an overall heat

loss coefficient can be calculated for the gasification unit by matching the predicted temperatures against the measured temperatures.

However, it is difficult to accurately validate theoretical heat loss calculations because gasifiers contain extremely high temperatures and environments that are at first oxidizing then reducing, corrosive, and erosive. For large diameter gasifiers it is difficult to maintain thermocouples that are long enough to reach the core of the gasifier thus it is challenging to measure the exact temperature profile in gasifiers (Basu, Acharya, & Dutta, 2010).

#### 2.4 Effect of Bed Temperature on the Quality of Syngas

The temperature of the gasifier bed affects all of the chemical reactions involved in the gasification process. As was previously stated, the temperature of the bed is influenced by the oxidation and reduction reactions, the initial temperatures of the feed streams, and the amount of heat loss to the surroundings. Thus it is important when modeling a gasifier that the amount of heat loss is accurately calculated since the internal temperature will affect the overall syngas composition.

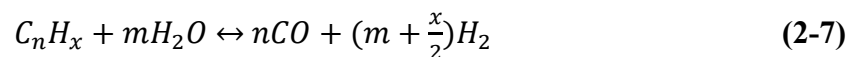
In an experiment conducted by Narváez et al. (1996), an increase in gasifier bed temperature from 700 °C to 850 °C, at a constant equivalence ratio (ER) of 0.30, the composition of the raw gas produced was altered: the H<sub>2</sub> content increased from 5 to 10% by volume, CO increased from 12 to 18% by volume, CO<sub>2</sub> decreased from 16 to 14% by volume. Methane and C<sub>2</sub>H<sub>2</sub> decreased minimally. The results from a similar experiment conducted by Radmanesh et al. (2006) validated the conclusions drawn from Narváez et al. (1996) in that when the temperature

of the gasifier bed is increased and the ER is held constant, the concentrations of H<sub>2</sub> and CO in the syngas increased.

From Petersen and Werther's (2005) study on a circulating fluidized bed gasifier using sewage sludge as the fuel, a large change in syngas composition was observed with an increase in bed temperature from 530 to 730 °C at an ER of 0.30. The H<sub>2</sub> to CO ratio doubled over this temperature range. However at temperatures above 730 °C, Petersen and Werther did not see significant syngas composition changes with increasing temperatures (Petersen & Werther, 2005).

In a sewage sludge gasification experiment from de Andrés et al. (2011), it was shown that higher bed temperatures favor hydrogen production and that the concentration of CH<sub>4</sub> increases slightly with increasing bed temperatures. Higher temperatures produce more intense volatilizations and cracking reactions instead of producing more intense reforming reactions. Thus at higher temperatures there is an increase in H<sub>2</sub> and light hydrocarbons in the syngas (de Andrés et al., 2011). This pattern is shown for temperature ranges of 750-850 °C at constant ERs of 0.20, 0.30, and 0.40.

Tar content also decreases as temperature increases. This is a result of increased tar cracking (Equation 2-6) and steam reforming (Equation 2-7) reactions of the types shown below (de Andrés et al., 2011; Manyà et al., 2006; Narváez et al., 1996).



Where

C<sub>n</sub>H<sub>x</sub> = tar compound

These changes in composition affect the overall heating value and quality of the gas. An increase in bed temperature, up to a point, increases the heating value and decreases the tar content which makes for a better quality syngas. Figure 2-3 illustrates the effect of temperature on heating value, tar content, char conversion, and sintering for different fuels used in fluidized-bed gasification. Note that increased bed temperature could have positive effects on the syngas quality (lower tar content) but could also be detrimental to the amount of energy produced (lower heating value). Experimental literature has shown that increases in temperature in sewage sludge gasifier-bed improve the heating value of the gas until the temperature reaches 1470 °F for a bubbling fluidized-bed (BFB) gasifier and 1340 °F for a circulating fluidized-bed (CFB) gasifier (Kang et al., 2011; Petersen & Werther, 2005).

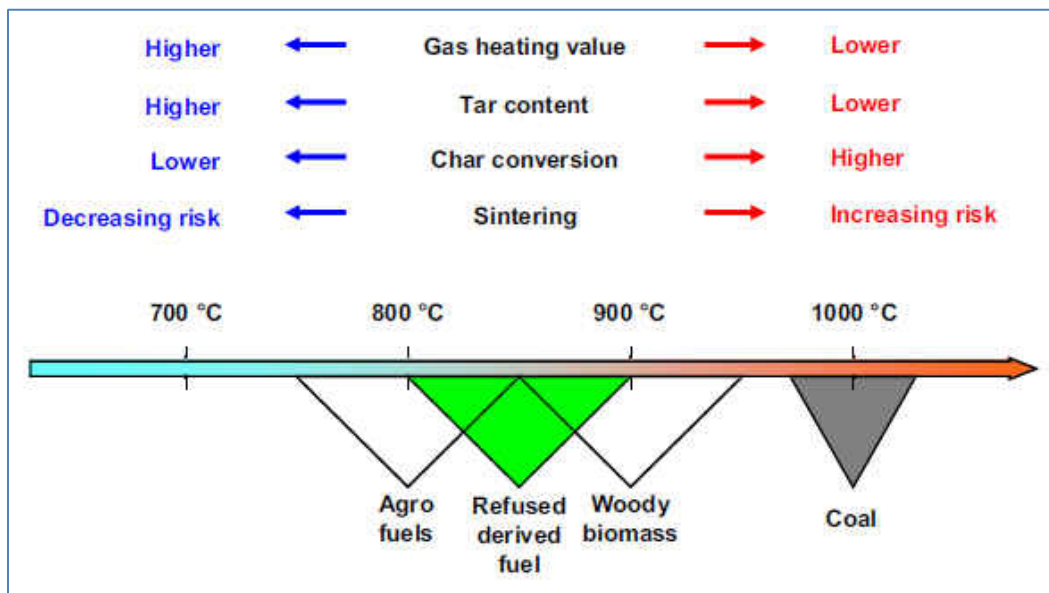


**Figure 2-4. Effect of Temperature on Parameters and Processes during Gasification (Adapted from Gómez-Barea et al., 2013)**

One way to potentially avoid the temperature constraints created by the tradeoffs shown in Figure 2-4 is to physically separate gasification into three stages: fluidized bed devolatilization, non-catalytic air/steam reforming (removal of tars) from the gas exiting the devolatilization zone, and filtering of the gas and char generated in the devolatilizer (Gómez-Barea, Leckner, Perales, Nilsson, & Cano, 2013).

The FLETGAS system used in the laboratory experiment conducted by Gómez-Barea et al. (2013) consisted of a (1) devolatilizer, a (2) reformer, and (3) a moving bed (see Figure 2-5). The devolatilizer is where most of the volatile gases are released from the biomass, and was operated at temperatures in the range of 700-750 °C which are high enough to release the volatile gases from the sewage sludge but not high enough to cause any tar cracking so a significant amount of tar was released from the fuel in the devolatilizer. The tar and syngas was directed to another stage downstream of the devolatilization zone called the reformer. Oxygen-enriched air (40% O<sub>2</sub>) and high temperature steam was blown into the reformer to greatly reduce the amount of tars by raising the temperature in the reformer to 1200 °C which partially combusted the tars. The solids (char and ash) produced in the fluidized bed were then transferred to the third stage, the moving bed. The reformer gases flowed into and transferred heat to the moving bed. The bed acted like a catalytic filter in promoting tar decomposition reactions while steam introduced into the bed promoted endothermic char gasification reactions. Finally, the ashes exited the bottom of the moving bed containing very little carbon and the syngas exited near the bottom of the moving bed containing negligible amounts of tar due to the two reduction steps encountered in the process. The final stage of the system, the moving bed, cooled the ash and syngas streams which increased the chemical energy of the syngas and thus the overall gasification efficiency.

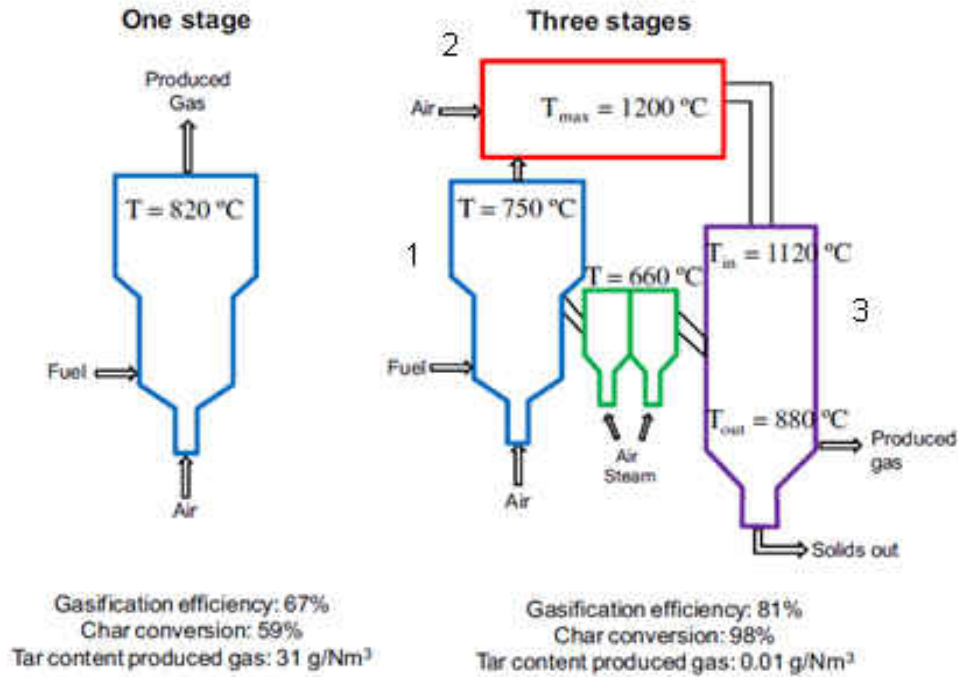


**Figure 2-5. Comparison between a Single-Stage FBG and a Three-Stage FBG System (FLETGAS) for Sewage Sludge Gasification (Adapted from Gómez-Barea et al., 2013)**

As can be seen in Figure 2-5, the three-stage method for gasification is more efficient for sewage sludge gasification than the one-stage method. The three stages also produce a higher char conversion so not as much carbon is left in the ash. A lower tar content allows for fewer downstream removal treatments which can be a complex and expensive process.

## 2.5 Effect of Equivalence Ratio on Syngas Quality

The equivalence ratio (ER) is defined as the ratio between the flow rate of the air introduced into the reactor and the stoichiometric flow rate of the air required for complete combustion of the fuel (see Equation 2-8). It has also been stated in the literature that it is one of

the most important operational variables in biomass gasification (Narváez et al., 1996; Petersen & Werther, 2005).

$$ER = \frac{O_2 \text{ Supplied}}{\text{Theor. } O_2 \text{ Required}} \quad (2-8)$$

Where:

$O_2$  Supplied = Mass flow rate of free oxygen into the gasifier (lbs/hr)  
Theor.  $O_2$  Required = Theoretical amount of oxygen needed for complete combustion of feedstock (lbs/hr)

ER greatly affects the syngas composition. As ER increases, the concentrations of combustible gases ( $H_2$ , CO,  $CH_4$ , and tars) decrease while the concentrations of  $CO_2$  and  $H_2O$  increase. Increases in ER provide more  $O_2$  to the gasifier which then goes to oxidize CO,  $H_2$ ,  $CH_4$ , and tars. The methanation and oxidation reactions use  $O_2$  to oxidize  $CH_4$  to CO and  $H_2$ ; hydrogen is oxidized to  $H_2O$ . This trend can be seen in the literature over temperature ranges of 700-850 °C for both biomass and sewage sludge fuel (de Andrés et al., 2011; Liu & Gibbs, 2002; Manyà et al., 2006; Narváez et al., 1996; Petersen & Werther, 2005; Radmanesh, Chaouki, & Guy, 2006).

Recommendations in the literature for an optimal ER vary based on feed stock and type of gasifier. In Petersen and Werther's (2005) experiment using sewage sludge as a fuel and a circulating bed gasifier, the optimal ER was found to be 0.30. Narváez et al. (1996) recommends values between 0.18 and 0.45 for the ER in their experiment using biomass as a fuel and a bubbling fluidized bed gasifier. A lower ER is not practical because too much tar is produced and a higher ER produces a syngas with a low heating value. In Manyà et al.'s (2005) experiments with a dried sewage sludge fed fluidized bed gasifier, an optimal ER was found at

0.35; the “optimum” qualification was determined by the highest concentration of H<sub>2</sub> in the syngas.

## 2.6 Use of Temperature as a Fitting Parameter

Validation of developed kinetic computer models is a major challenge because data from commercial gasifiers are scarce (for confidentiality concerns) and very few commercial gasifiers have the ability to sample and test the syngas on a routine basis. If they are equipped with gas sampling ports they are generally located after the gas cleaning station. By the time the syngas reaches the cleaning station it has cooled down considerably and might have undergone further chemical and/or physical changes (such as tar condensation) thus changing the composition of the gas from when it exited the gasifier (Basu & Kaushal, 2009). One of the only parameters that can be measured accurately is the temperature at various places inside of the gasifier. The temperature profile inside the gasifier is usually an output from gasifier models.

In an experiment with a fluidized bed biomass gasifier, Kaushal, Proll, and Hofbauer (2007) compared the predicted temperature of the gasifier with the measured temperature at three different heights in the riser: dense, middle, and upper zones. The predicted temperature was less than five degrees Kelvin over the measured temperatures which the author considered to be in good agreement (Kaushal et al., 2007). In another experiment with a circulating fluidized bed biomass gasifier, Miao et al. (2014) compared the model prediction of axial temperature gradient with the actual temperature profile. The results of the model were about 30 °C higher than the actual temperature data which was considered a reasonably close agreement. The maximum discrepancy between the experimental data and the model occurred at the feeding point of the gasifier. This discrepancy could have been attributed to the assumption in the model that the fuel was fed from the bottom of the gasifier when in actuality it was fed from some height above the



bottom of the gasifier bed. The fuel entered the gasifier and underwent fast pyrolysis which absorbed large amounts of heat leading to a low recorded temperature while the model did not account for this effect (Miao et al., 2014).

### 3. MAXWEST BIOSOLID GASIFICATION PROCESS

#### 3.1 Overview of Operations

At the MaxWest facility located at the City of Sanford Wastewater Treatment Plant in Sanford, Florida, sludge (5-15% solids) is brought in from several wastewater treatment plants and is stored in a tank. The wet sludge is then dewatered by a belt filter press, dried in a specially designed dryer, and is then stored until enough biosolids has been accumulated to operate the gasifier. The dryer system accepts biosolids at an average of 25% solids (75% water) and dries them to about 90% solids. The biosolids dryer is heated by hot oil coming from the heat exchanger located after the thermal oxidizer. Once the biosolids are dried they are moved to a holding bin and then to a feed bin before being fed into the gasifier. The biosolids enter the gasifier at 6.3 feet above the bottom of the unit at an average temperature of 120 °F (see Figure 3-1).

The gasifier system is a MW2000 model (see Figure 3-1) and is operated at an average biosolid feed rate of 1038 lb/hour. Biosolids enter the fluidized bed 6.3 feet from the bottom of the unit while a mixture of hot flue gas and ambient air is blown in 3.3 feet below the biosolids feed port. At the bottom of the gasifier is a layer of silica sand which provides a fluidizing medium and rapidly heats the biosolids. The sand has a bulk density of 2.63 g/m<sup>3</sup> (unfluidized) and occupies the space between the bottom of the gasifier and the bottom of the biosolid feed port. After the air starts flowing, the bed expands to an approximate height of 6 feet.

The gasifier system is a bubbling fluidized-bed which provides efficient contact between the fuel particles and the air. The temperatures achieved in the gasifier when operated at the above mentioned feed and air rates range between 1200 °F in the bottom of the gasifier and 1090

°F in the upper portion. The sand in the bottom keeps the temperatures relatively constant while in the upper portion of the gasifier, with no sand, the syngas experiences significant heat loss. Higher temperatures around 1450 °F can cause unwanted ash agglomeration (MaxWest Environmental Systems, Inc., 2013).

## Gasifier Design

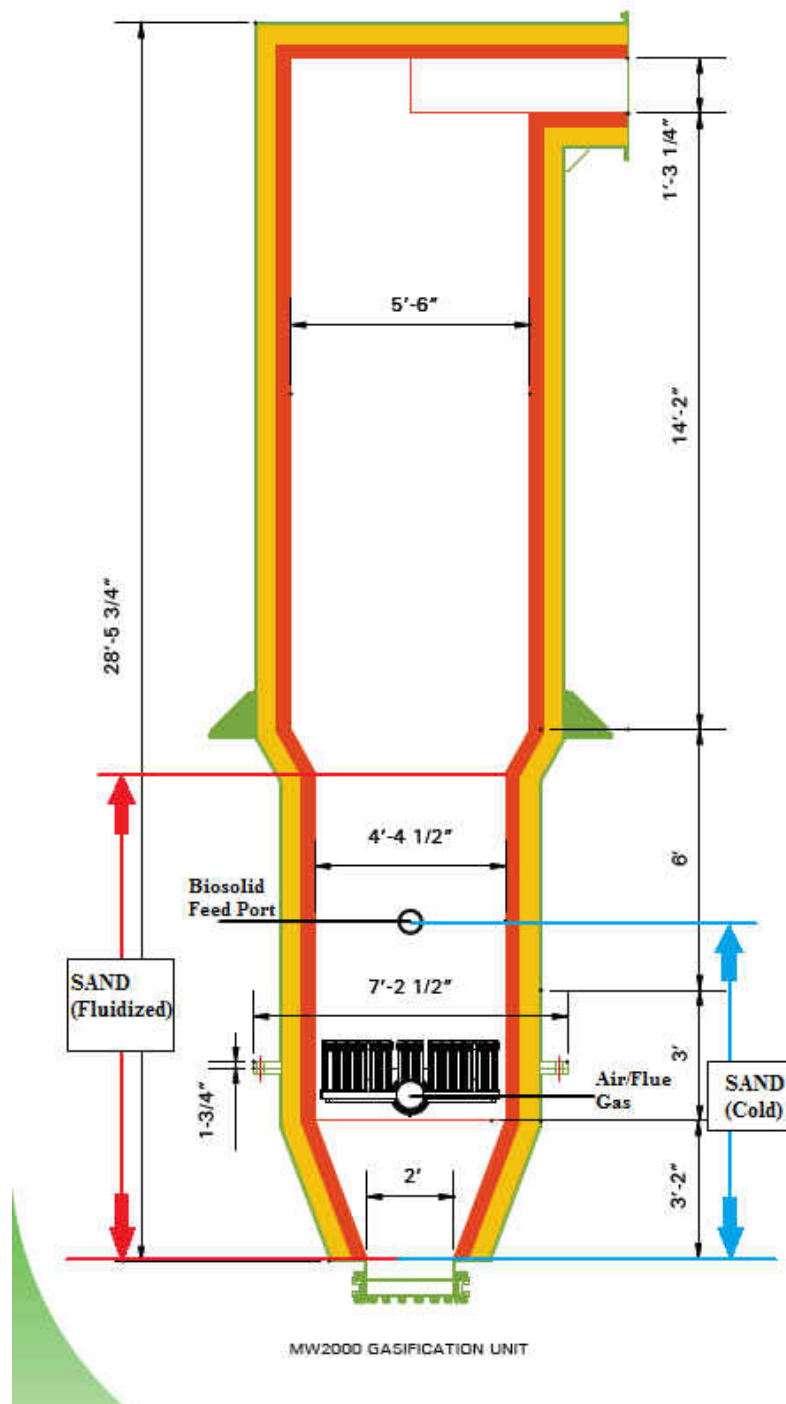


Figure 3-1. MW2000 Gasification Unit (Adapted from MaxWest Environmental Systems, Inc., 2012)

At the MaxWest facility, a mixture of air and flue gas from the thermal oxidizer is fed into the bottom of the gasifier. The flue gas used in the fluidized bed gasifier is diverted from the cooling stack located after the heat exchanger. Recycled flue gas is used (1) to increase the velocity in cyclone, especially when using a lower biosolid feed rate, (2) to control the temperature in the gasifier, and (3) to prevent excessive combustion of the fuel (because of its small concentration of oxygen). On average, the ratio of flue gas to ambient air used is about 5.6 (flue gas) to 1 (ambient air), each measured in pounds per hour. This higher ratio of flue gas, which contains mostly nitrogen (71%), water vapor (10.9%), carbon dioxide (8.8%) and oxygen (8.1%), to ambient air, which contains significantly more oxygen (21%), is to keep the environment inside the gasifier near pyrolysis state (limited oxygen) thus preventing excessive combustion and elevated temperatures.

The syngas and ash that is formed in the gasifier is then transported out of the top of the gasifier into the cyclone. The syngas exits the gasifier at an average of 1090 °F. The 32 inch diameter cyclone removes the majority of the ash from the syngas and empties it into two ash augers and then into two large ash bins which are emptied into a truck and taken to the landfill. The cleaned syngas leaves the cyclone at about 975 °F and is transported to the thermal oxidizer.

The syngas then enters the thermal oxidizer at an average temperature of 875 °F. The thermal oxidizer operates with two air rings that supply a mixture of ambient air and recycled flue gas from the exhaust stack to combust the syngas. The oxidizer is also equipped with an aqueous ammonia injection port to control nitrous oxide emissions. The combusted gas exits the thermal oxidizer at an average temperature of 1560 °F and enters the heat exchanger.

The thermal oxidizer exhaust gas (flue gas) flows through a heat exchanger where oil is heated and the flue gas is cooled. As an example of the operation of the heat exchanger, the following temperatures were taken from one steady-state run: the heat exchanger raises the temperature of the oil from 500 °F to 534 °F, while cooling the flue gas from 1570 °F to 585 °F. The hot oil is then pumped back to the biosolids dryer to facilitate moisture removal.

The use of the two step process, gasification of the fuel and then combustion of the syngas in a separate device, allows for more control over NO<sub>x</sub> formation within the oxidizer. The first air ring limits the amount of oxygen (substoichiometric), making oxygen unavailable to form NO<sub>x</sub>, and the second air ring completes the combustion of the syngas (Santoleri et al., 2000). The two step process also allows for more control over particulate matter. The cyclone first removes the majority of the particulate matter before the syngas is combusted and then the baghouse and wet scrubber remove the finer particulate matter.

MaxWest employs air pollution control (APC) devices downstream of the heat exchanger. These include a hot filter baghouse and a wet scrubber. The baghouse removes finer particles that the cyclone could not remove. The wet scrubber uses an average of 100 gallons per minute of treated effluent and then sends that water back to the head of the wastewater treatment plant. The cleaned exhaust gas from the wet scrubber flows to the exhaust stack (some of the flue gas exits into the atmosphere and some is recycled back to the gasifier or thermal oxidizer-see Figure 3-2).

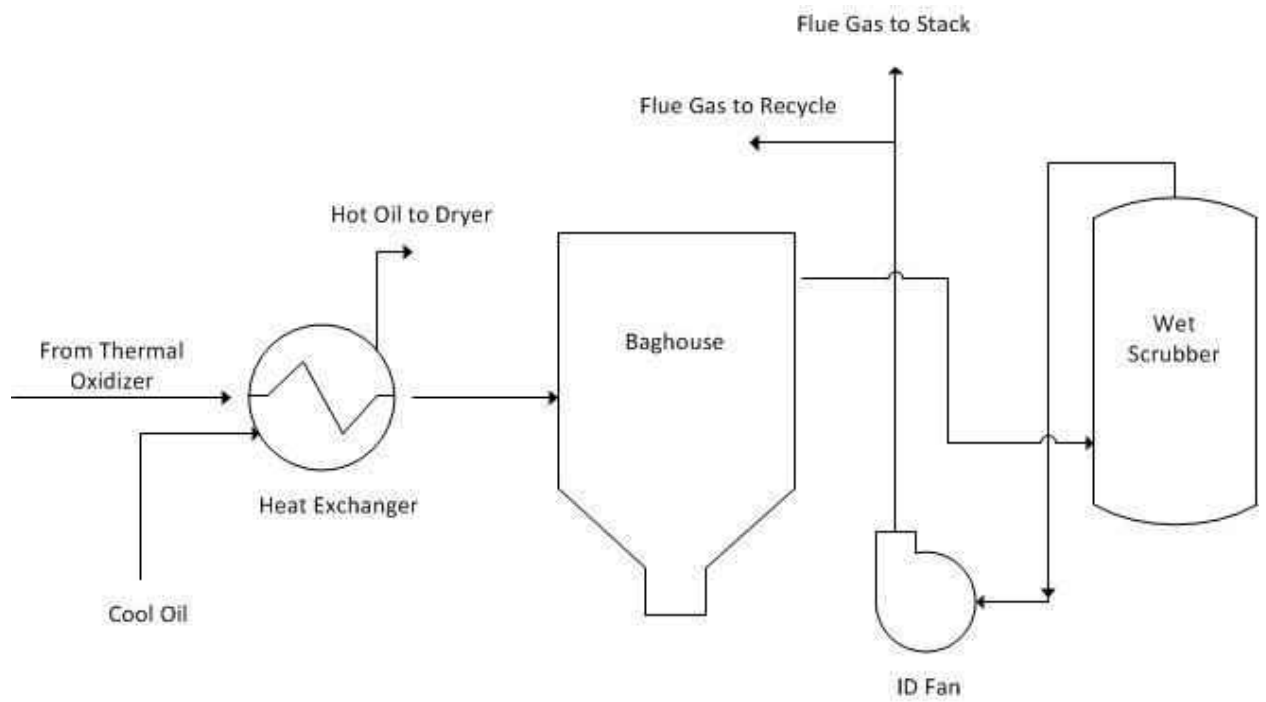
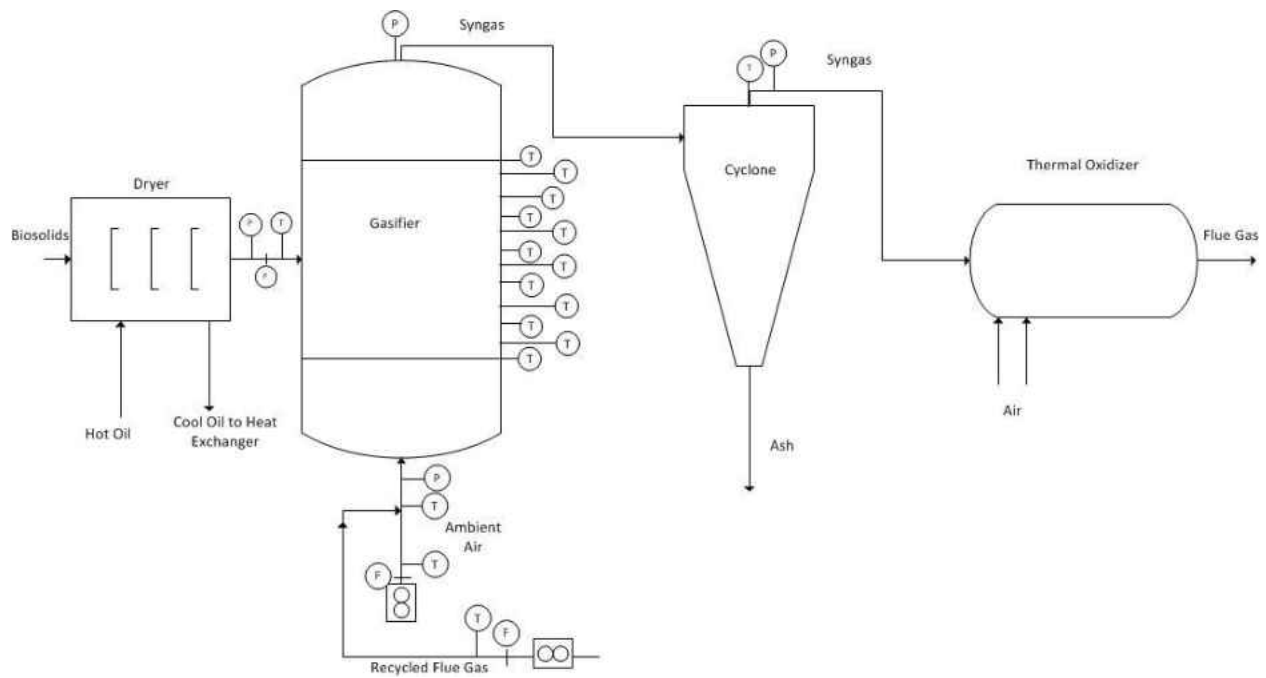


**Figure 3-2. MaxWest Process Equipment**

### 3.2 Data Collection Process

Six trips were made out to the MaxWest facility in Sanford, Florida, to collect operating data from the gasifier system. The main data of interest were the dry solids feed rate into the gasifier, the temperature of the dry solids, the rate of recycled flue gas and ambient air entering the fluidized bed, their respective temperatures, and the temperature profile throughout the entire gasifier. Enough data were collected on these trips to compile a base case for the MaxWest gasification system. The Tables 3-1 and 3-2 tabulate averaged data taken from ten steady-state runs from January 28, 2014 to April 24, 2014.

Questions about the typical operational parameters were directed to Paul Cairney, Chief Operating Officer at MaxWest, Robert Macklin, Engineer, Anthony Martinez, Plant Operator, Charleston Jarvis, Plant Operator, and Irmarié Aguiar, Technical Administrator.

The gasification system has several temperature probes, flow rate meters, and pressure probes on their equipment and ducts (see Figure 3-2). The data collected by these instruments are recorded and saved in the company's Historian. The temperature probes along the gasifier are thermocouples going up each side of the gasifier. The probes in the bottom half of the gasifier are 10 inches apart while the probes in the upper half are 11 inches apart. For research purposes, temperature data were only collected from the right side of the gasifier since the data from the left side were identical.

Specific data collected from the MaxWest Historian system were compiled and averaged (see Tables 3-1 and 3-2). Data for each measurement device were collected every minute (some devices such as air flow rate were collected several times per minute) over a steady-state run (where the biosolid feed rate was held stable) and were averaged for every hour during that



specific run. Data for a total of 10 steady-state runs were collected and then averaged together. This final data set was used as the default input data for the computer model.

**Table 3-1. Base Case Operation Data \***

| Biosolid Feed Rate (lb/hr) | Temperature of Biosolids (°F) | Flow Recycled Flue Gas (lb/hr) | Temperature of Flue Gas (°F) | Flow Ambient Air (lb/hr) | Temperature of Ambient Air (°F) |
|----------------------------|-------------------------------|--------------------------------|------------------------------|--------------------------|---------------------------------|
| 1038                       | 322                           | 1742                           | 319                          | 311                      | 294                             |

\*Average of 10 steady-state runs during January to April, 2014.

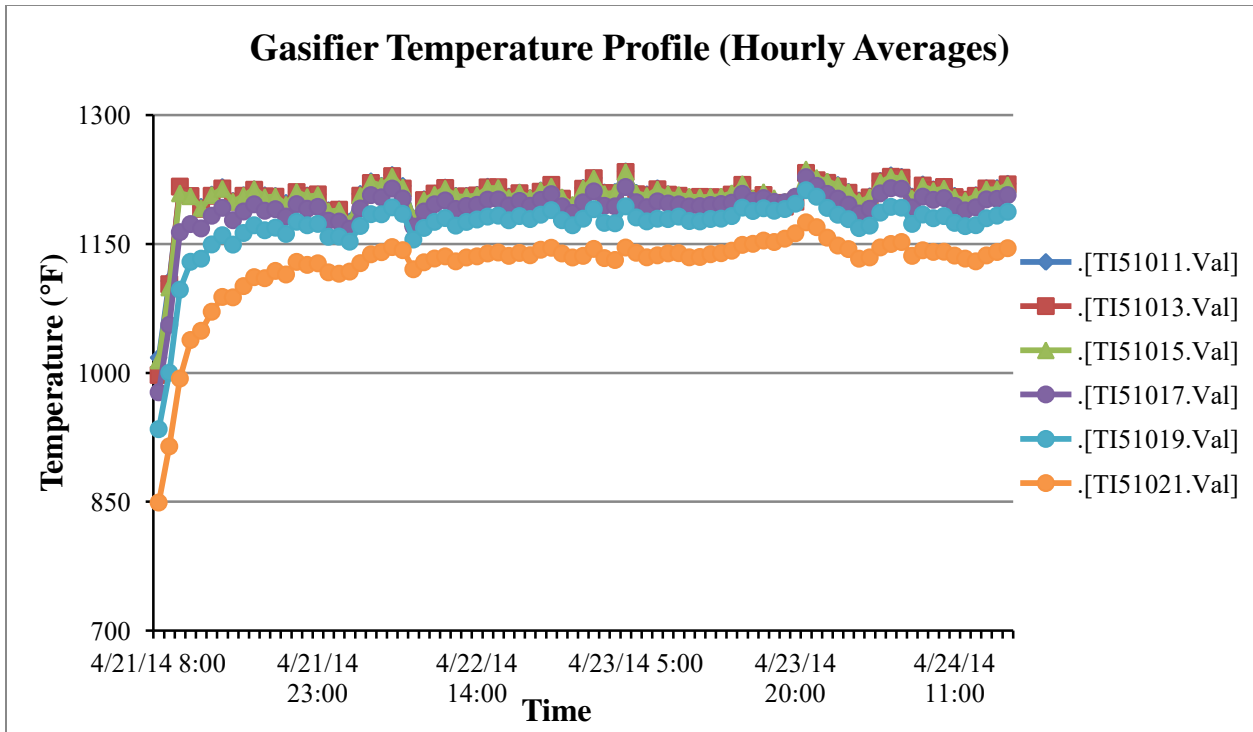
**Table 3-2. Base Case Gasifier Temperature Profile\***

| Location from Biosolid Feed Port (inches) | Internal Gasifier Temperature (°F) |
|---|------------------------------------|
| 129.6                                     | 1094                               |
| 118.6                                     | 1132                               |
| 107.6                                     | 1155                               |
| 96.6                                      | 1171                               |
| 85.6                                      | 1187                               |
| 74.6                                      | 1199                               |
| 63.6                                      | 1211                               |
| 53.6                                      | 1211                               |
| 43.6                                      | 1212                               |
| 33.6                                      | 1211                               |
| 23.6                                      | 1221                               |
| 13.6                                      | 1207                               |

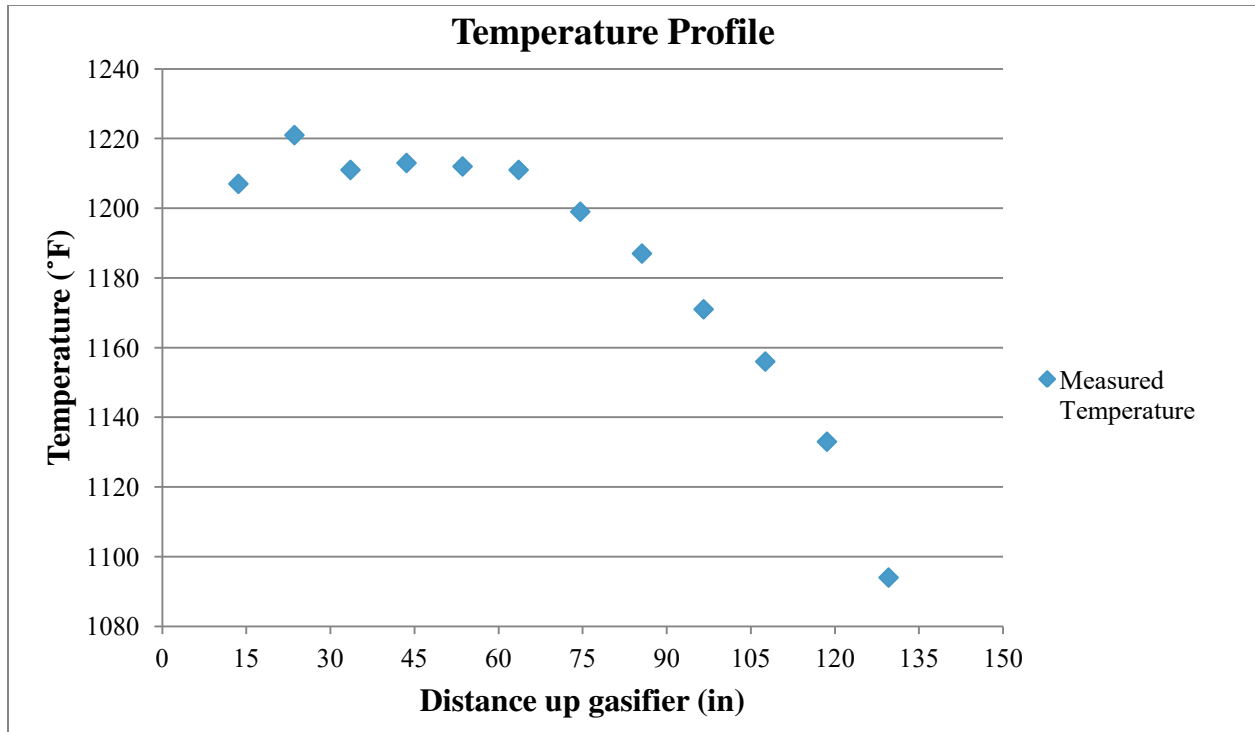
\*Average of 10 steady-state runs during January to April, 2014.

Figure 3-3 shows the steady-state temperatures within the gasifier during a run which started April 21, 2014, and continued through April 24, 2014. Each symbol represents a specific temperature probe on the gasifier; TI51011 is the bottom temperature probe on the gasifier and is located 13.6 inches above the center of the biosolid feed port (see Figure 3-1). TI51021 is the top probe on the gasifier and is located 129.6 inches (10.8 feet) above the center of the biosolid feed port. The graph shows that the temperatures within the gasifier decrease as the height of the measurement increases. This is particularly evident in the upper two probes (TI51019 and TI51021) which are located in the freeboard area of the gasifier. The lower probes are located in the fluidized-bed portion of the gasifier where the fluidizing agent, silica sand, keeps the temperature profile relatively constant.

Figure 3-4 illustrates the temperature profile throughout the gasifier at one time during the run in April, 2014. It is evident that the fluidized portion of the bed (13.6 inches to 72 inches in height) has a relatively stable temperature which is caused by the heat carried in the fluidized sand. Above the fluidized bed is the freeboard where a significant amount of heat loss occurs.



**Figure 3-3. Gasifier Steady-State Temperatures**



**Figure 3-4. Temperature Profile in Gasifier**

### *3.2.1 Determination of Density of Gasifier Sand*

Two 200-gram samples of the silica sand used in the fluidized bed gasifier at the MaxWest facility were collected to determine its bulk density. In the Geotechnical Laboratory at the University of Central Florida, a guide written by Robert Slade (2010) was used, along with the help of Juan Cruz, to determine the specific gravity of the sand.

First the mass of an empty 500 mL volumetric flask was measured (186.6 grams) and then the flask was filled up to the 500 mL line with distilled water. Next the new weight of the flask and water and was measured and the temperature of the water was recorded (685.3 grams and 25.5 °C respectively).

The emptied and dried flask was then filled with 100 grams of dry silica sand and the new mass was recorded (286.6 grams). Then enough distilled water was added to fill the flask about 2/3 of the way from the fill line. A vacuum pump was applied to the flask for five minutes to remove air from the voids in the soil. Once the voids were removed, the flask was filled to the 500 mL mark with distilled water and the new weight was measured (747.3 grams).

This process was repeated a second time with results differing by less than 0.3%.

The following calculations were performed to calculate the specific gravity and specific density of the silica sand:

$$M_s = W_B - W_A \quad (3-1)$$

Where:

$$M_s = \textit{Weight of sand}$$

$$W_B = \textit{Weight of sand and flask}$$

$$W_A = \textit{Weight of flask and water}$$

$$M_s = 286.6 \textit{ g} - 186.6 \textit{ g} = 100 \textit{ g}$$

$$M_w = (M_1 + M_s) - M_2 \quad (3-2)$$

Where:

$$M_w = \textit{Weight of water}$$

$$M_1 = \textit{Weight of water and flask}$$

$$M_s = \textit{Weight of sand}$$

$M_2 = \text{Weight of sand and flask and water, no voids}$

$$M_w = (685.3 \text{ g} + 100 \text{ g}) - 747.3 \text{ g} = 38 \text{ g}$$

$$G_{S(T^\circ C)} = \frac{M_s}{M_w} \quad (3-3)$$

Where:

$G_{S(T^\circ C)} = \text{Specific gravity at measured temperature}$

$$G_{S(25.5^\circ C)} = \frac{100 \text{ g}}{38 \text{ g}} = 2.63158$$

$$G_{S(20^\circ C)} = G_{S(T^\circ C)} * A \quad (3-4)$$

Where:

$A = \text{Temperature adjustment factor at } 25.5^\circ C$

$$G_{S(20^\circ C)} = 2.63158 * .9987 = 2.628$$

The specific density of the silica sand was evaluated as shown below:

$$\rho = 2.628 * 1000 \frac{\text{kg}}{\text{m}^3} * 1000 \frac{\text{g}}{\text{kg}}$$

$$\rho = 2.63 * 10^6 \frac{\text{g}}{\text{m}^3}$$

The results from this experiment agree with the literature values for the density of silica sand ( $2.1 \times 10^6 \text{ g/m}^3$ ) (Densities of Miscellaneous Solids).

## 4. DETERMINATION OF HEAT LOSS COEFFICIENT

### 4.1 Temperature Profile Comparison

Axial profiles of temperature throughout the gasifier are very important because all kinetic constants in the gasification reactions depend on temperature. To calculate the concentration of a gaseous specie at some height in the gasifier, the temperature at that height has to be known. Temperature profile comparison was chosen as the method to validate the gasifier computer model developed by Champion et al. (2014). The original computer model developed by Champion et al. (2014) will be referred to as M1. No syngas compositional data were available for this research. These data would have provided a much more robust method for validating the model because the reaction kinetics could be more accurately modified so that the final syngas composition more closely matched the measured composition.

The gasifier model (M1) output denotes temperatures for each CSTR (ten in total) in the expanded bed zone of the gasifier. The expanded bed of the gasifier contains the fluidizing sand and is where the oxidation and gasification reactions occur. The theoretical expanded bed height was estimated to be 72 inches in height and 52.5 inches in diameter. The ten CSTRs are assumed to be identical in size so each temperature generated in the model was assumed to occur every 7.2 inches for a total of 10 temperatures throughout the gasifier bed (Champion et al., 2014). These data were used to make a temperature profile graph to which the actual temperature profile measured at the MaxWest facility could be compared. The thermocouple distances were 10 inches apart for the lower portion of the gasifier and 11 inches apart for the upper portion for a total of 12 temperatures. The thermocouple probes reached just beyond the inside walls of the gasifier, not into the core of the unit.



When M1 was initially run with the base case data that was averaged from data collection trips to MaxWest (see Table 3-1), the modeled temperatures were consistently higher than the measured temperatures. To have M1 more closely match the temperature activity of the physical gasifier, several things were tried. The first thing was to determine the exact density of the silica sand used in the MaxWest gasifier. The details of the density determination were given in Section 3.1.1. This did not improve the model temperatures significantly. Increasing the heat loss percentage assumed in M1 was then attempted but this did not lower the temperatures noticeably. Even when the input heat loss was raised from 5% (the default) to 50% the modeled temperature profile remained higher than the measured temperatures. The decision was then made to implement heat loss as a coefficient specific to the MaxWest gasifier instead of modeling heat loss as an overall percentage.

#### 4.2 Heat Loss Calculations and Determination of Heat Loss through Freeboard

A heat loss coefficient was determined for the MaxWest gasifier using temperature data and gasifier physical dimensions collected at the operational facility. A specific heat capacity ( $C_{p_i}$ ) was calculated for every component of the syngas, using molar heat capacity coefficients from Santoleri Reynolds, & Theodore (2000), measured temperatures from the upper portion of the gasifier, and Equation 4-1.

$$C_{p_i} = \frac{(\alpha_i*(T_2-T_1) + \frac{\beta_i}{2}*(T_2^2-T_1^2) + \frac{\gamma_i}{3}*(T_2^3-T_1^3))}{\Delta T} \quad (4-1)$$

Where:

$Cp_i = \text{specific heat capacity for gas } i \left( \frac{\text{Btu}}{\text{lbmol}\cdot^\circ\text{F}} \right)$

$\alpha_i, \beta_i, \gamma_i = \text{molar heat capacity coefficients}$

$T_2 = \text{temperature leaving zone in gasifier (K)}$

$T_1 = \text{temperature entering zone in gasifier (K)}$

$\Delta T = T_2 - T_1 \text{ (}^\circ\text{F)}$

An overall average heat loss coefficient (U) was then calculated for the gasifier using the previously calculated specific heat capacities and molar flow rates from the model using Equation 4-2. The area of one CSTR zone in the gasifier was calculated as 61.92 ft<sup>2</sup> (diameter of 54.54 inches, and height of 11 inches). Measurements were taken from engineering drawings of the unit.

$$U = \frac{\Delta H}{A \cdot \Delta T} \quad (4-2)$$

Where:

$U = \text{heat loss coefficient} \left( \frac{\text{Btu}}{\text{ft}^2\text{-hr}\cdot^\circ\text{F}} \right)$

$\Delta H = \text{change in enthalpy of gas stream} \left( \frac{\text{Btu}}{\text{hr}} \right)$

$A = \text{outside wall area of zone in gasifier (ft}^2\text{)}$

$\Delta T = \text{difference between temperature entering zone and temperature leaving zone}$

A final overall heat loss coefficient was calculated as 9.43 J/m<sup>2</sup>-s-K. Instead of applying a percentage to the heat exiting each CSTR, the revised model now calculates the heat loss in each CSTR using Equation 4-3. The area of each CSTR was calculated as 3.96 m<sup>2</sup> and the ambient temperature was assumed to be 85 °F (302 K). The revised model at this stage of development will be referred to as M2.

$$\text{Heat loss } (qL) = U * A * \Delta T \quad (4-3)$$

Where:

$$qL = \text{heat loss } \left(\frac{J}{s}\right)$$

$$U = \text{heat loss coefficient } \left(\frac{J}{m^2 \cdot s \cdot K}\right)$$

$$A = \text{area of theoretical CSTR } (m^2)$$

$$\Delta T = \text{difference between gasifier temperature and ambient temperature } (K)$$

This new method of calculating heat loss improved the modeled temperature profile significantly, and M2 more closely modeled the actual temperature profile observed in the MaxWest gasifier. More importantly, it allows the model to predict the temperature loss that occurs in the freeboard.

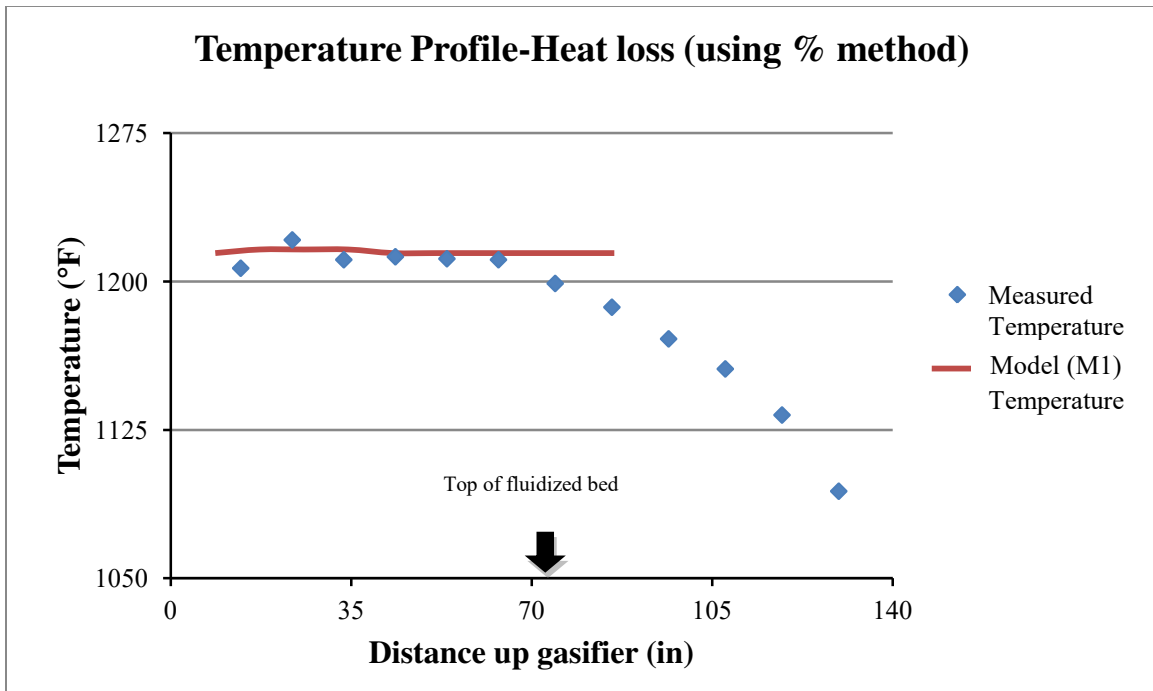
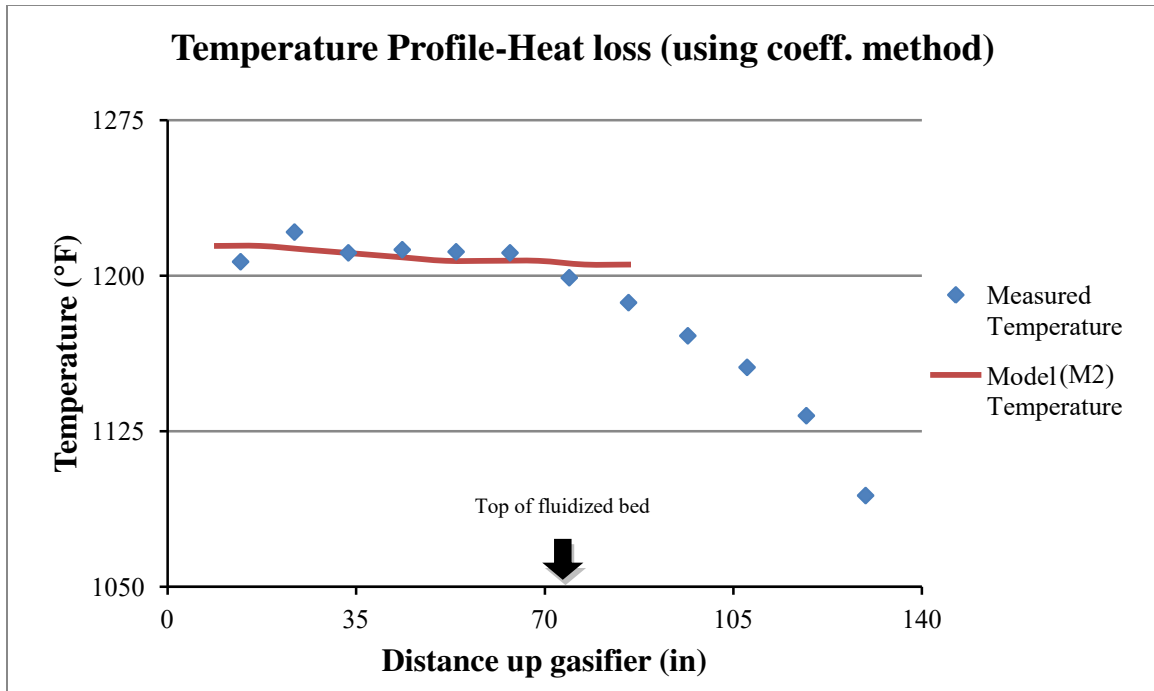


Figure 4-1. Temperature Profile Comparison using Heat Loss as a Percentage (model M1)



**Figure 4-2. Temperature Profile Comparison using Heat Loss Coefficient (model M2)**

Figure 4-2 shows the temperature profile from the model using the aforementioned heat loss coefficient method. It shows that this method of heat loss estimate provides a more accurate representation of the actual measured temperature profile.

The most significant portion of the profile that does not match up is at the top of the fluidized bed. The measured temperature shows a more significant decrease in temperature than is predicted by the model. Significant heat loss occurs in the gas phase (freeboard) after the oxidation and reduction reactions are completed. This heat loss can be seen in Figure 4-2 where the measured temperature decreases by about 100 °F after the top (end) of the fluidized bed. M1 did not account for heat loss in the area between the fluidized bed and the top of the gasifier (Champion et al., 2014).

Further heat loss calculations were put into the model code to account for the heat loss experienced in the freeboard of the gasifier (see Equation 4-4). The final output syngas temperature is now the temperature of the syngas leaving the gasifier and not the temperature of the syngas leaving the final CSTR in the gasifier bed. The average heat capacity was calculated by averaging the heat capacities of the syngas components (O<sub>2</sub>, CO, CO<sub>2</sub>, H<sub>2</sub>, CH<sub>4</sub>, H<sub>2</sub>O, C<sub>6</sub>H<sub>6</sub>, NH<sub>3</sub>, HCl, H<sub>2</sub>S, N<sub>2</sub> and Ar) which were calculated using Equation 4-1 over the temperature range 1048-1105 °F. This is the average temperature range recorded for the upper area of the gasifier.

$$T_{i+1} = T_i - \frac{(U \cdot A \cdot (T_i - T_{ambient}))}{(\dot{n}_{gas} \cdot C_{p \text{ avg}})} \quad (4-4)$$

Where:

$T_{i+1}$  = temperature leaving zone in gasifier (K)

$T_i$  = temperature entering zone in gasifier (K)

$U$  = heat loss coefficient ( $\frac{J}{m^2 \cdot s \cdot K}$ )

$A$  = heat transfer area of upper portion of gasifier (m<sup>2</sup>)

$C_{p \text{ avg}}$  = average heat capacity of final syngas composition ( $\frac{J}{gmol \cdot K}$ )

$\dot{n}_{gas}$  = molar flow rate of syngas ( $\frac{gmol}{s}$ )

The bottom of the gasifier is relatively insensitive to changes in the heat loss coefficient due to the heat capacity of the sand in the fluidized bed. The upper portion of the gasifier does not have the temperature influence of the sand and all of the heat is either carried by the gas or is

lost through the walls of the gasifier. By varying  $U$  and plotting results from the model, it was discovered that a heat loss coefficient of  $4.0 \text{ J/m}^2\text{-s-K}$  provided a good temperature profile match with the collected data from the MaxWest facility (see Figure 4-3). This improved model, distinguished by the addition of a revised heat loss coefficient and extension to the freeboard zone, will be referred to as M3.

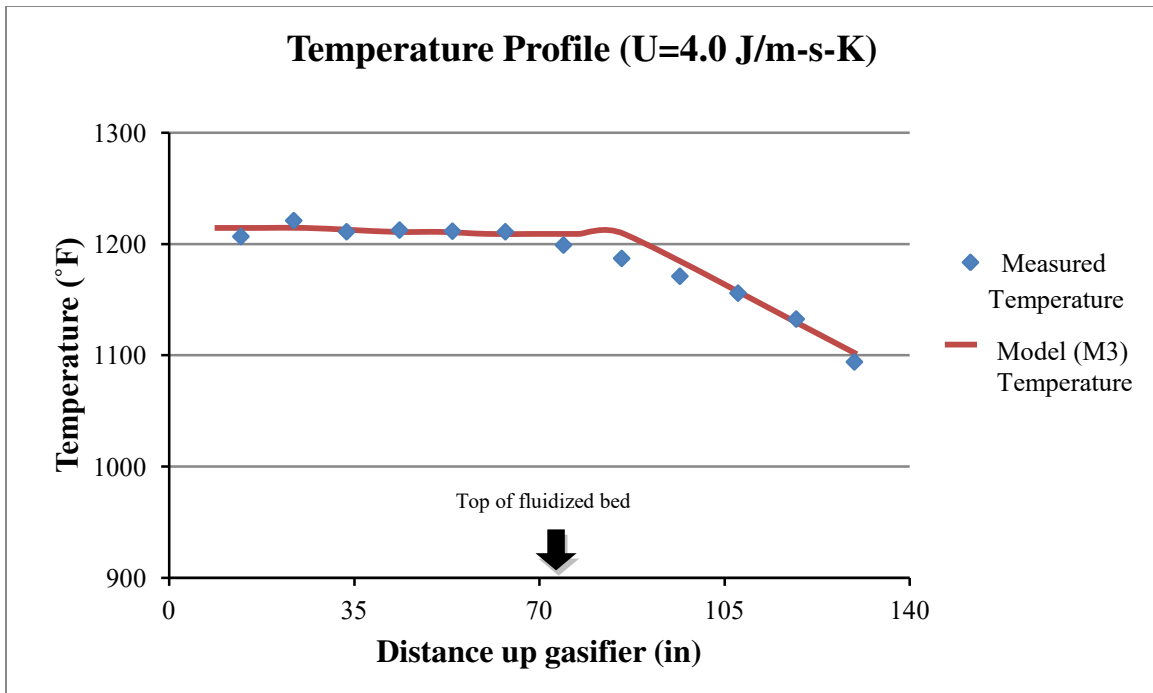


**Figure 4-3. Temperature Profile Comparison with Heat Loss Coefficient =  $4.0 \text{ J/m-s-K}$  (model M3)**

## 5. SENSITIVITY ANALYSIS

### 5.1 Changing Reaction Kinetics

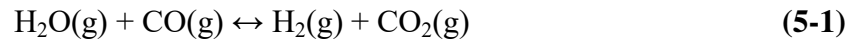
This author decided to adjust some of the reaction kinetic constants to try to further improve M3. Prior to changing the reaction kinetics, the behavior of syngas composition with changes in ER or temperature did not match the literature well. The literature shows that with increasing temperature, at a constant ER, the concentration of CO<sub>2</sub> decreases and the concentration of CO increases (de Andrés et al., 2011; Narváez et al., 1996; Petersen & Werther, 2005; Kang et al., 2011; Radmanesh et al., 2006). This pattern was not evident in the predicted syngas composition so the kinetic constants of two reactions (Boudouard and water-gas shift) were modified from the original values in M1 to obtain results closer to those seen in the literature (de Andrés et al., 2011; Narváez et al., 1996; Kang et al., 2011; Radmanesh et al., 2006).

The Boudouard and water-gas shift reaction were chosen to be adjusted because they involve the production of CO and CO<sub>2</sub> (Petersen & Werther, 2005). Also, these reaction rates were among some of the rates that were significantly modified by Champion et al. (2014). As previously mentioned, the change in syngas composition with increasing bed temperature contradicted the literature in that in the model (M1) the concentration of CO<sub>2</sub> increased with increasing temperatures and the concentration of CO decreased which was the opposite of what was observed in the literature. The reaction constants for the Boudouard and water-gas shift reactions were modified back to their original literature values as is explained below. By slowing down the water-gas shift reaction and increasing the rate of the Boudouard reaction, it was theorized that the concentration of CO in the syngas would increase and the trend between

CO/CO<sub>2</sub> with increasing bed temperature would more closely match what was seen in the literature.

### 5.1.1 Water-Gas Shift Reaction

The water-gas shift reaction is a gasification reaction that involves the reduction of H<sub>2</sub>O to produce H<sub>2</sub> (see Equation 5-1) along with the oxidation of CO.



The rate expression for the water-gas shift reaction is represented by Equation 5-2 (Petersen & Werther, 2005):

$$r_6 = k_6 * e^{\frac{-12,560 \text{ J/mol}}{RT}} \left\{ [\text{CO}][\text{H}_2\text{O}] - \frac{[\text{CO}_2][\text{H}_2]}{K_6} \right\} \quad (5-2)$$

Where:

$$K_6 = 0.022 * e^{\frac{34,730 \text{ J/mol}}{RT}}$$

$$k_6 = 2.78 \times 10^{-1}$$

Champion et al. (2014) determined that the pre-exponential term for the water-gas shift reaction ( $k_6$ ) should be slowed by a factor of 10 in order to create a model that reasonably matched some experimental results that they found in the literature. This change was explained by stating that the kinetic constants found in the literature were derived from other types of biomass including wood and rice husks, not sewage sludge and that the experiments took place at higher temperatures, in shock-tubes, so it was assumed that the environment of a gasifier would lead to much slower oxidation of tars. The final pre-exponential value used by Champion et al. (2014) was  $2.78 \times 10^{-2}$ .



### 5.1.2 Boudouard Reaction

The Boudouard reaction is also a gasification reaction and is important in the formation of CO from solid char and CO<sub>2</sub> (see Equation 5-3).



The rate expression for the Boudouard reaction is represented by Equation 5-4 (Petersen & Werther, 2005):

$$r_6 = k_6 * e^{\frac{-12,560 \text{ J/mol}}{RT}} \left\{ [\text{CO}][\text{H}_2\text{O}] - \frac{[\text{CO}_2][\text{H}_2]}{K_6} \right\} \quad (5-4)$$

Where:

$$K_6 = 0.022 * e^{\frac{34,730 \text{ J/mol}}{RT}}$$

$$k_6 = 3.18 \times 10^7$$

Champion et al. (2014) also changed the pre-exponential term for the Boudouard reaction ( $k_6$ ); it was decreased by a factor of 100 for the reasons described in section 5.2.1. The final pre-exponential value used by Champion et al. (2014) was  $3.18 \times 10^5$ .

After the modifications to the Boudouard and water-gas shift reaction rates as well as modifications to other reaction rates by Champion et al. (2014), the syngas composition data fit within the 2:1 and 1:2 slope lines on scatterplots. The scatterplots compared literature syngas composition to model output for temperatures of 1380-1560 °F and ER or 0.20-0.40 (de Andrés et al., 2011; Kang et al., 2011; Manyá et al., 2006). These model (M1) validation experiments depicted by the scatterplots assumed a gasifier heat loss of 5.0% and were conducted over a relatively small temperature range (1380-1560 °F) (see Figures 5-4, 5-6, 5-8, and 5-10).

Although Champion et al. (2014) saw a good fit between literature and model syngas

composition, this was no longer the case when the lower end of the temperature range was expanded to 1100 °F and a heat loss coefficient of 4.0 J/m-s-K was employed. Also, when looking at a comparison of syngas composition (using M1) versus increasing bed temperature at a constant ER, there was no clear trend between CO/CO<sub>2</sub> and bed temperature which can now be seen with the aforementioned modifications to the Boudouard and water-gas shift reactions (see Figure 5-12).

The literature consistently shows when ER is held constant and bed temperature is increased, the CO production increases due to the incomplete combustion reactions and to the Boudouard and CO<sub>2</sub> reforming reactions (water-gas shift). Also CO<sub>2</sub> production slightly decreases, H<sub>2</sub> production increases, and the concentration of tars decreases due to cracking and steam reforming reactions (de Andrés et al., 2011; Narváez et al., 1996; Kang et al., 2011; Petersen & Werther, 2005; Radmanesh et al., 2006). With the pre-exponential kinetic constants chosen by Champion et al. (2014), the trends seen in the literature for CO/CO<sub>2</sub> concentrations were not seen in his model results. The M1 syngas output showed that with increasing temperature, CO production decreased while CO<sub>2</sub> production increased.

To improve these trends, the decision was made to change the pre-exponential terms for the water-gas shift and Boudouard reactions back to their original literature values (see Equations 5-2 and 5-4). These new values caused the trends in changes to the syngas composition with increasing temperatures to more closely match literature trends. This author will now refer to the model with the changes in pre-exponential terms for the Boudouard and water-gas shift reactions as M4. The model M4 produced the syngas composition depicted by Figure 5-8 which shows that with increasing bed temperature, the concentration of CO increases, CO<sub>2</sub> decreases, H<sub>2</sub> increases, and C<sub>6</sub>H<sub>6</sub> decreases.

Figures 5-1, 5-2, 5-3 show syngas composition predictions, for both M1 and M4, versus changes in bed temperature. Predictions of CO and CO<sub>2</sub> from M1 show a tapering off of these gases with increasing bed temperature while predictions from M4 show increasing CO and decreasing CO<sub>2</sub> with increasing temperature. Although M4 does not fit the experimental data as well as M1 (in Figures 5-4 through 5-11), the author believes M4 better predicts syngas composition because the trends seen in Figures 5-1 through 5-3 over wider temperature ranges more closely match the trends seen in the experimental data.

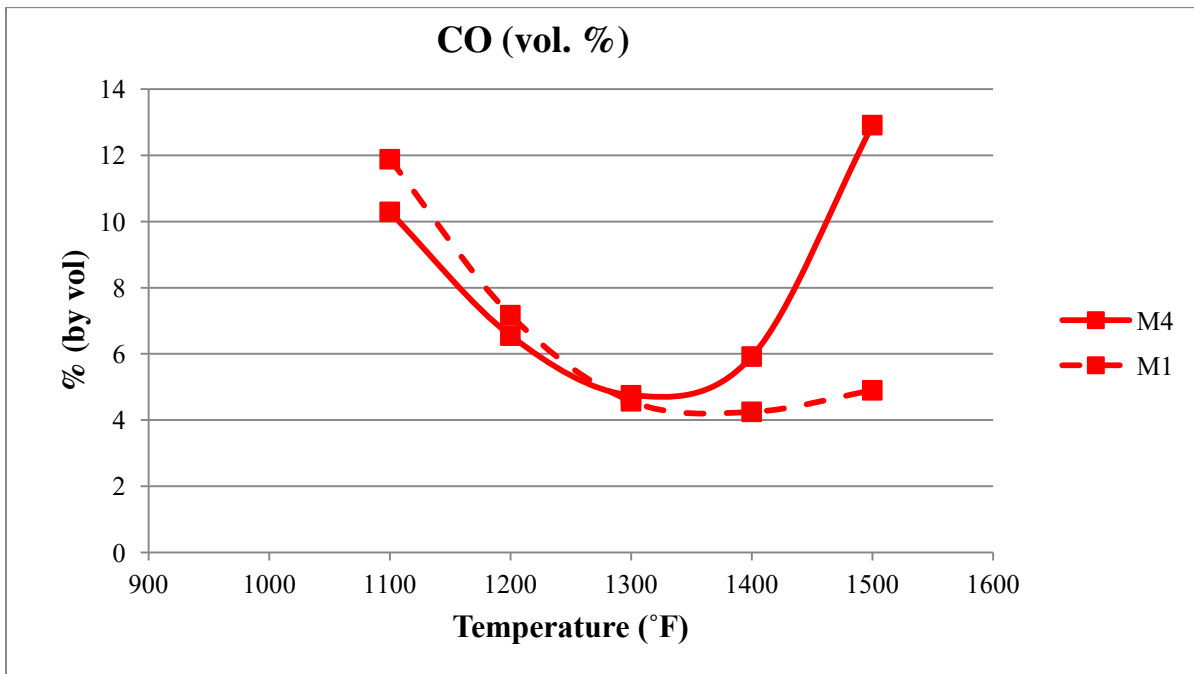


**Figure 5-1. CO Concentration vs Varying Temperature at ER=0.30**

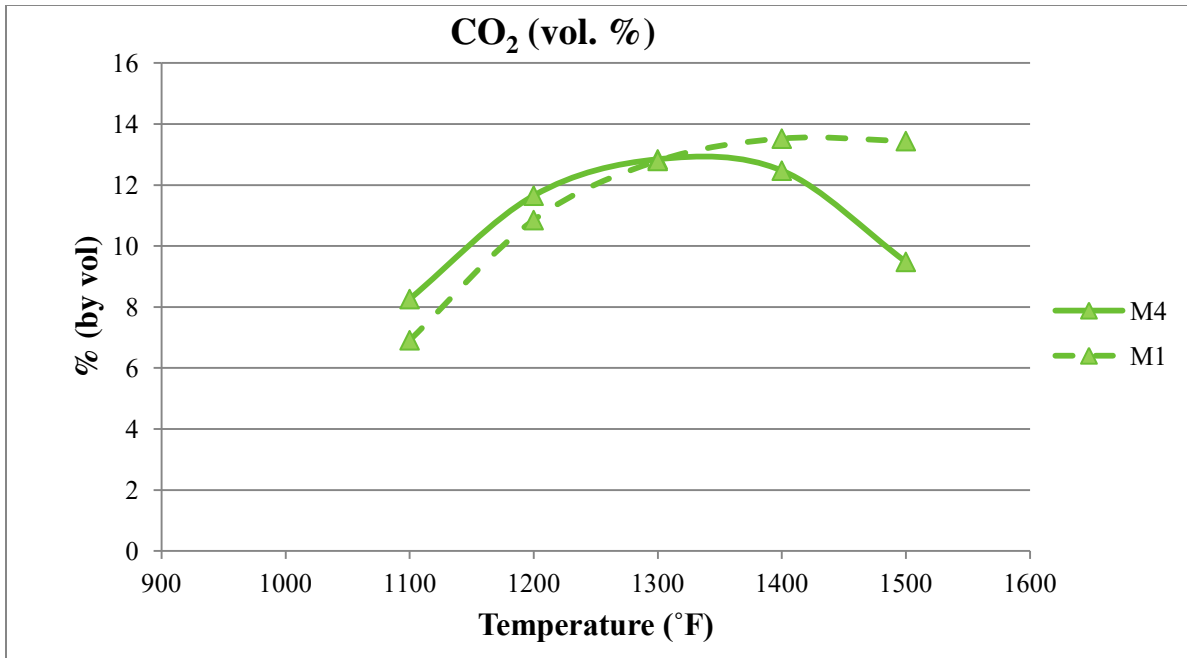


**Figure 5-2. CO<sub>2</sub> Concentration vs Varying Temperature at ER=0.30**

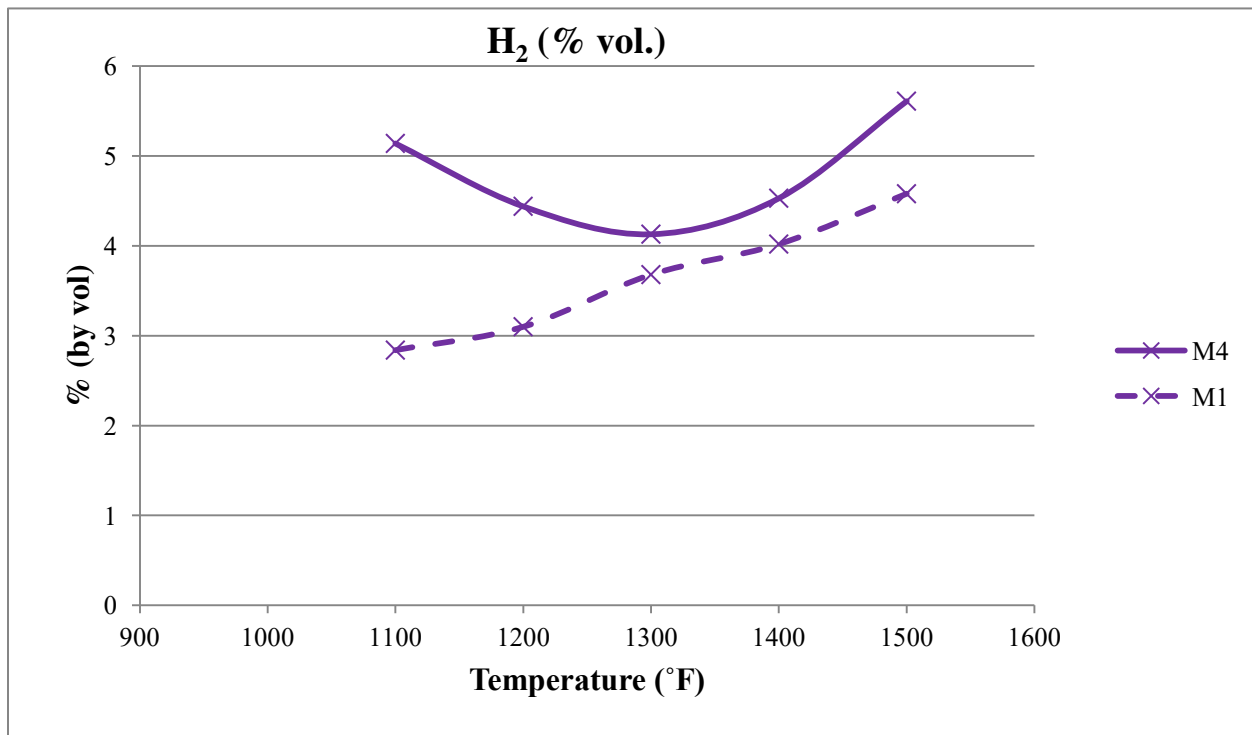


**Figure 5-3. H<sub>2</sub> Concentration vs Varying Temperature at ER=0.30**

Figures 5-4 through 5-11 show graphical comparisons between results from M1 (Figures 5-4, 5-6, 5-8, and 5-10) and M4 (Figures 5-5, 5-7, 5-9, and 5-11) and the literature sources (de Andrés et al., 2011; Kang et al., 2011; Manyá et al., 2006) for each of the principle gaseous species (CO, CO<sub>2</sub>, H<sub>2</sub>, and CH<sub>4</sub>). On these plots, the values on the x-axis represent normalized literature values, while the values on the y-axis represent normalized model-predicted values. The three other lines are 2:1 and 1:2 plots (upper and lower); the middle line is a 1:1 plot. If the model results compared exactly with the literature data, the points on the graph would fall on the middle (45°) line. If all points fall within the upper and lower lines, the model may be assumed to fit the literature data well.

The trends observed in Figure 5-5 show an over prediction of CO and the trends observed in Figure 5-7 show an under prediction of CO<sub>2</sub>. These predictions are a result of increasing the Boudouard reaction rate by a factor of 100. Although it appears that M4 is not predicting as well as M1, the overall predicted syngas trends (M4) over a wider temperature and ER range match well with the literature (de Andrés et al., 2011; Narváez et al., 1996; Kang et al., 2011; Petersen & Werther, 2005; Radmanesh et al., 2006).

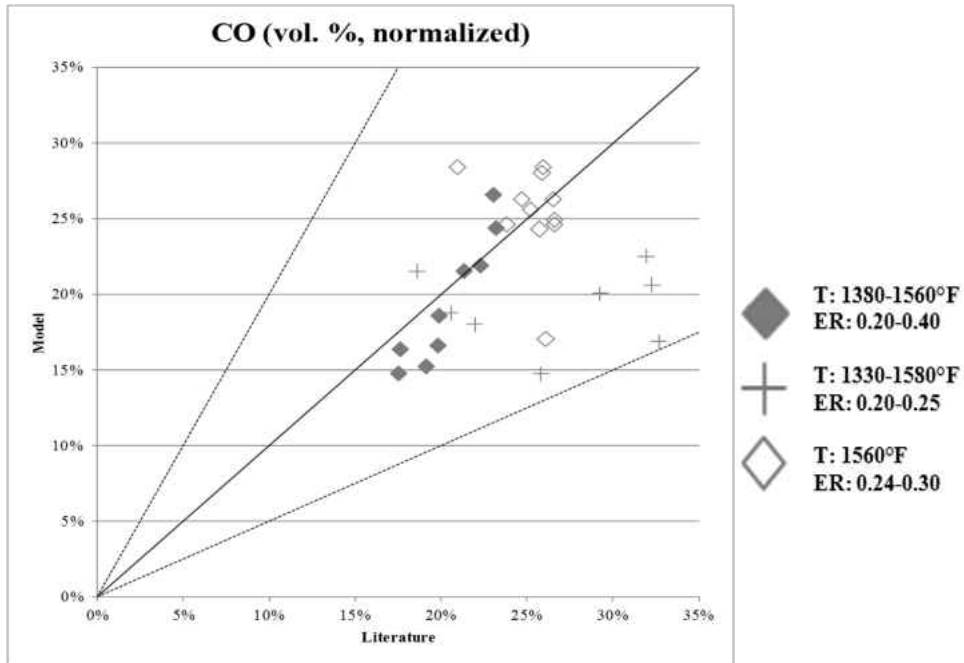


Figure 5-4. Comparison of Model (M1) Predictions (CO) with Literature

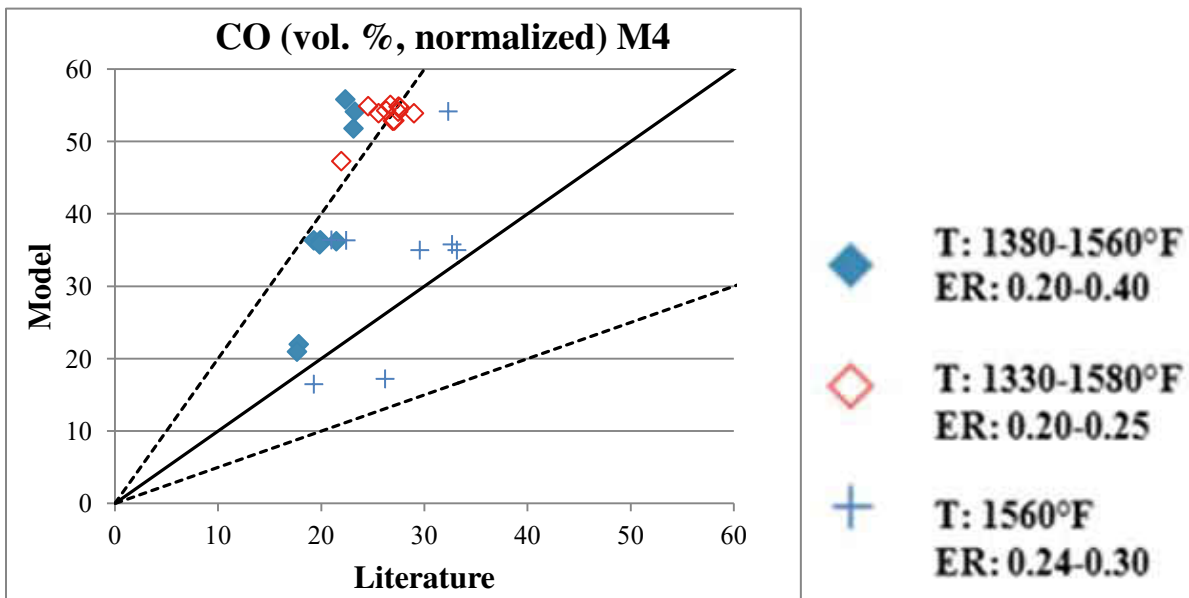


Figure 5-5. Comparison of Model (M4) Predictions (CO) with Literature

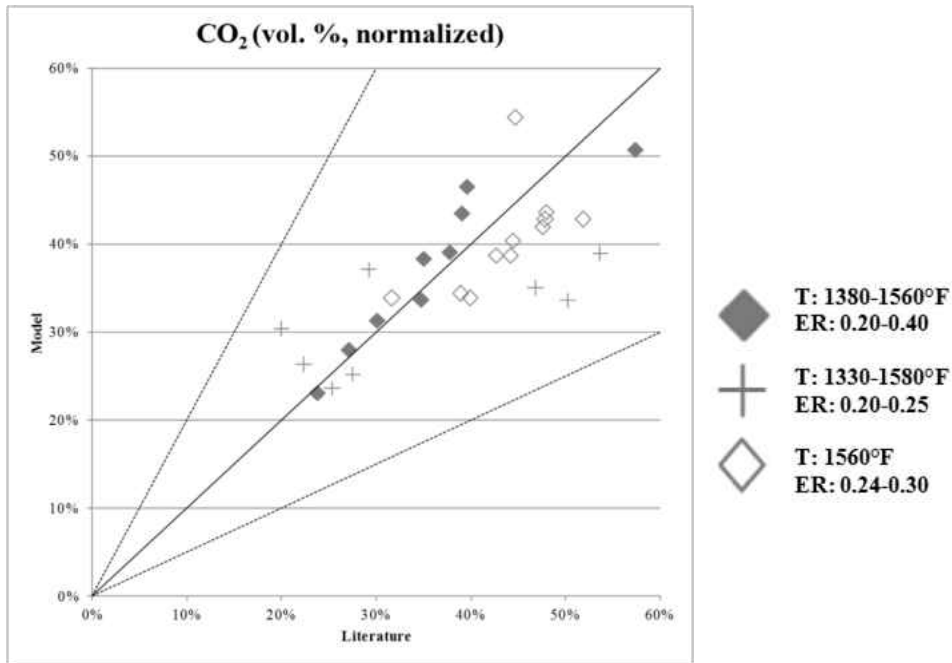


Figure 5-6. Comparison of Model (M1) Predictions (CO<sub>2</sub>) with Literature

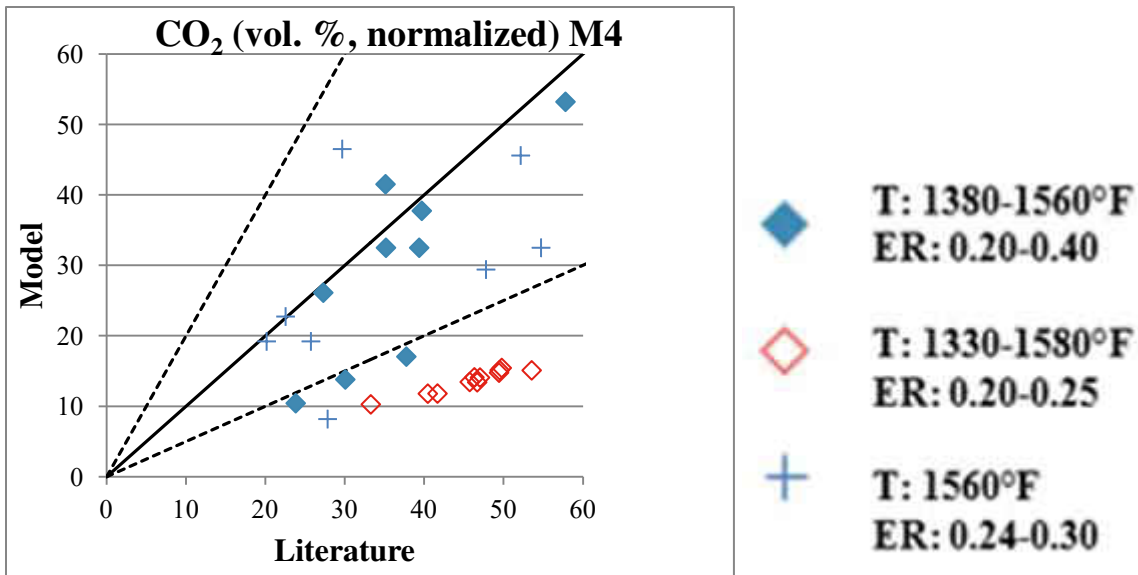


Figure 5-7. Comparison of Model (M4) Predictions (CO<sub>2</sub>) with Literature

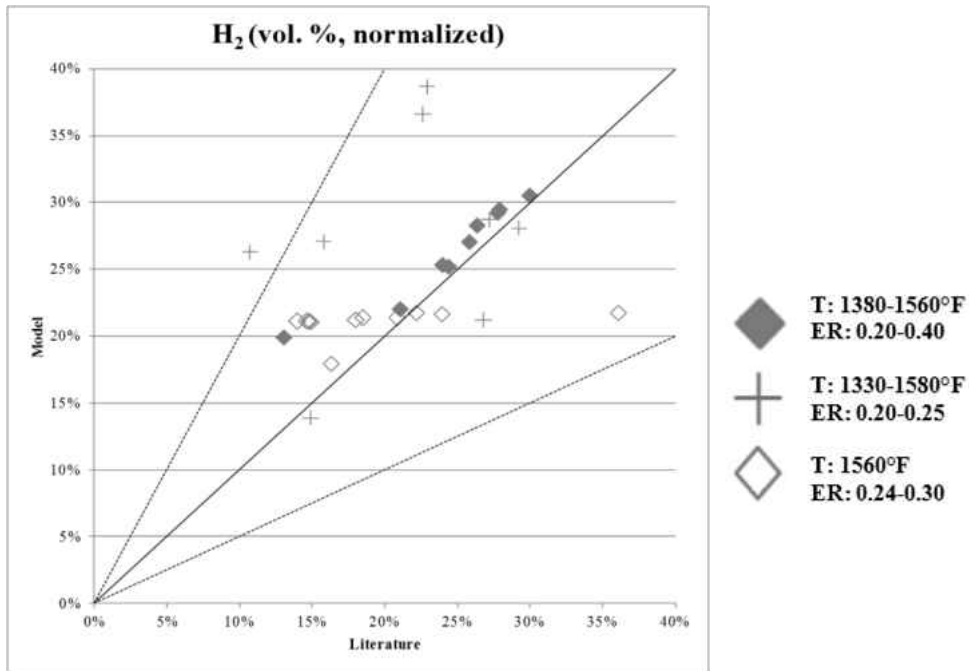


Figure 5-8. Comparison of Model (M1) Predictions (H<sub>2</sub>) with Literature

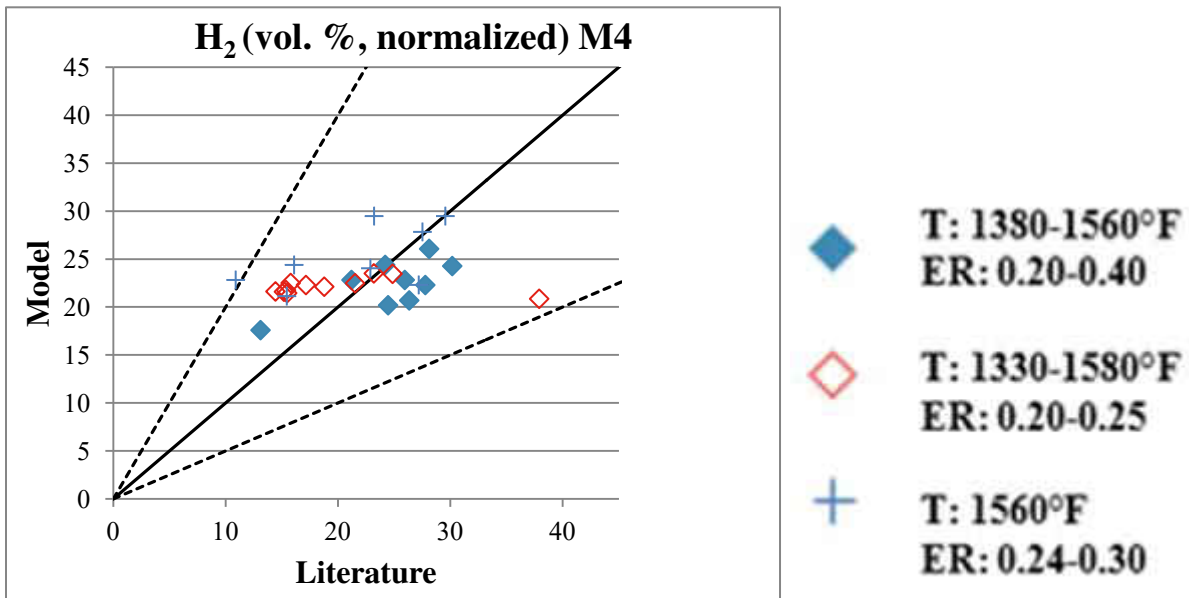


Figure 5-9. Comparison of Model (M4) Predictions (H<sub>2</sub>) with Literature



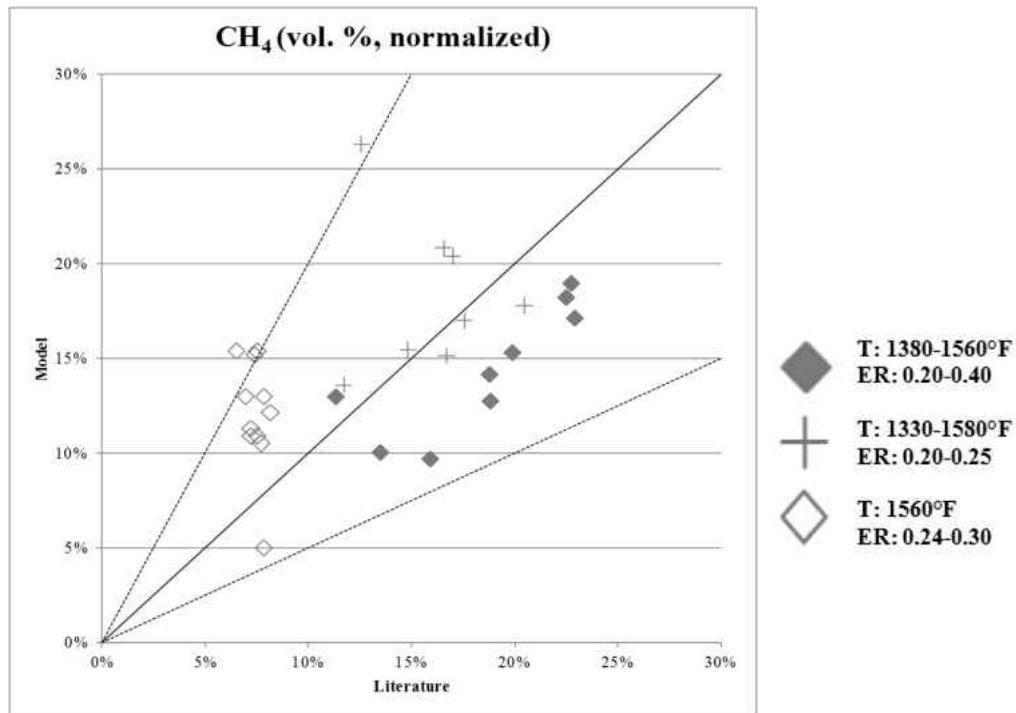


Figure 5-10. Comparison of Model (M1) Predictions (CH<sub>4</sub>) with Literature

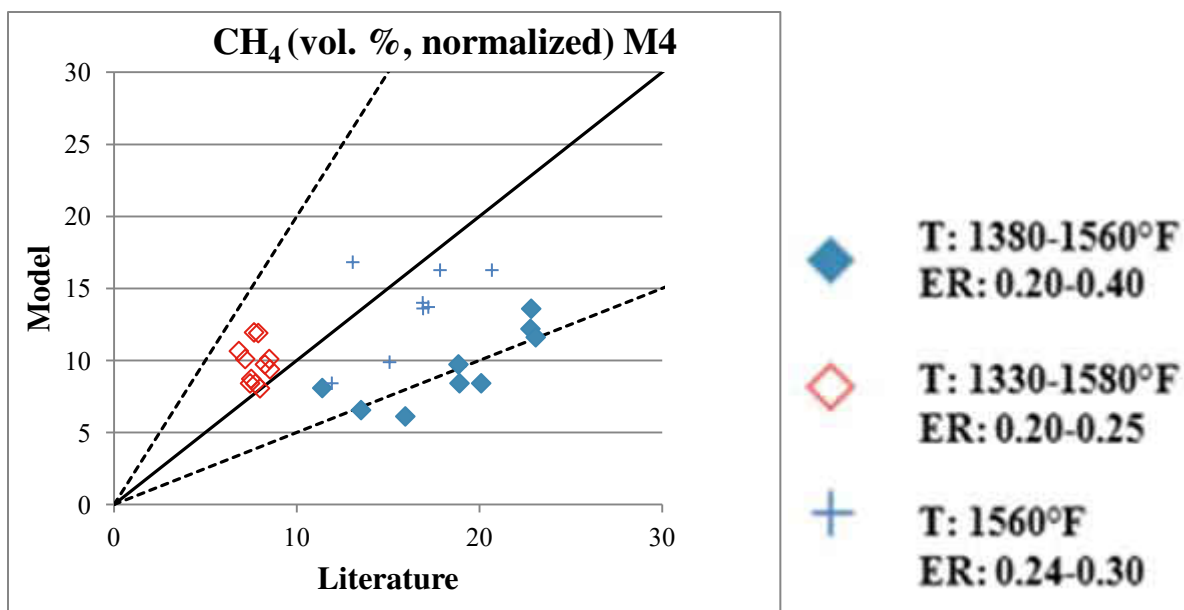
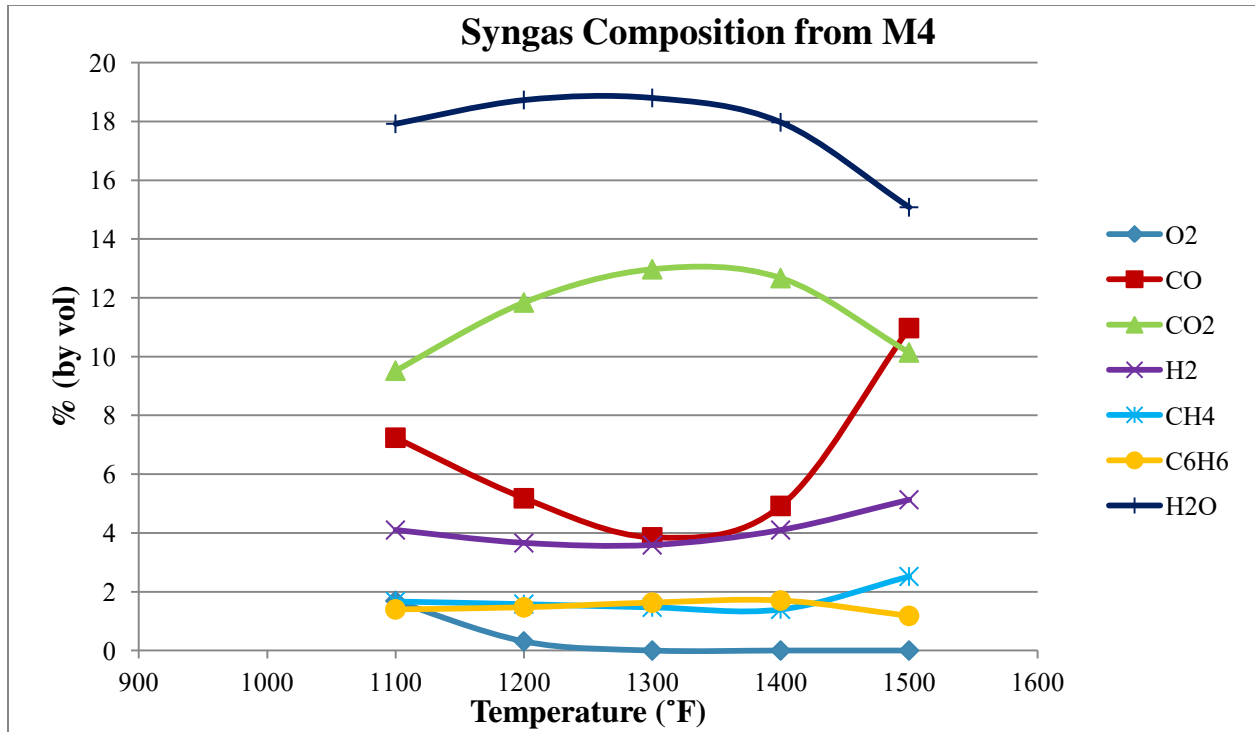


Figure 5-11. Comparison of Model (M4) Predictions (CH<sub>4</sub>) with Literature



**Figure 5-12. Syngas Composition with New Pre-Exponential Factors in Boudouard and Water-Gas Shift Reactions (at constant ER=0.21)**

### 5.2 Base Design Case Comparison

The syngas composition produced by M4 in the base case compares relatively well with the experimental results found in the literature (see Table 5-1). The base case input sewage sludge ultimate and proximate analysis were well within the range of selected literature experiments, and the model default ER was within the range (0.20-0.25) of the literature ER values. M4 predicted a smaller concentration of CO than was found in the experimental literature but this could be due to the lower bed temperature input (1300 °F) used in the base case model run. M4 also predicted higher concentrations of CO<sub>2</sub> compared to literature results, likely due to the lower bed temperature in the base case. The CO/CO<sub>2</sub> ratio increases with increasing temperature, so it is expected that a higher bed temperature will produce a syngas with higher

CO concentrations and lower CO<sub>2</sub> concentrations (de Andrés et al., 2011; Narváez et al., 1996; Kang et al., 2011; Radmanesh et al., 2006).

In M4, the predicted amount of CH<sub>4</sub> at 1300 °F was also lower than the average found in the literature (6.3% versus 8.7%). Champion et al. (2014) reduced the pre-exponential term for the methane oxidation reaction used in the model from its literature value because they found that the original value of that kinetic parameter caused rapid depletion of CH<sub>4</sub> concentrations.

**Table 5-1. Model (M4) Output Compared to Experimental Literature**

| Normalized Syngas Composition (% by volume) (ER = .20-.25) |           |                        |       |                    |                    |
|--|-----------|------------------------|-------|--------------------|--------------------|
|  | M4 Output | de Andrés et al., 2011 |       | Manyà et al., 2006 | Manyà et al., 2005 |
| CO   | 16.4%     | 19.1%                  | 23.0% | 25.0%              | 25.1%              |
| CO <sub>2</sub>  | 55.2%     | 37.7%                  | 29.2% | 42.3%              | 51.7%              |
| H <sub>2</sub>   | 15.3%     | 26.0%                  | 30.1% | 18.5%              | 14.2%              |
| CH <sub>4</sub>  | 6.3%      | 9.8%                   | 10.5% | 7.4%               | 6.9%               |
| Tars   | 6.9%      | 7.3%                   | 7.1%  | 6.8%               | 2.2%               |
| Bed Temperature (°F)                                       | 1300      | 1382                   | 1472  | Not Reported       | 1382               |

### 5.3 Delta Cases

#### 5.3.1 Varying Equivalence Ratio at Constant Temperature

The equivalence ratio (ER) is the ratio of the air provided to the stoichiometric air required for complete combustion of the fuel (see Equation 2-8).

When the ER is high, oxidation reactions are favored due to higher oxygen content in the fluidizing agent leading to greater amounts of CO<sub>2</sub> and smaller amounts of H<sub>2</sub> and CO. The increasing role of char combustion compared to gasification reactions results in lower concentrations of combustible gases and higher CO<sub>2</sub> (Radmanesh et al., 2006). The production of CH<sub>4</sub> and C<sub>6</sub>H<sub>6</sub> decreases as ER increases due to partial oxidation reactions (de Andrés et al, 2011). Tar concentration decreases as ER increases due to the oxidation of tars thus producing a cleaner syngas. Since a higher ER involves further oxidation of these combustible gases, the final syngas has a lower heating value.

The following oxidation and tar cracking reactions occur and are responsible for the decrease in CO, H<sub>2</sub>, CH<sub>4</sub>, and C<sub>6</sub>H<sub>6</sub> and the increase in CO<sub>2</sub> with an increasing in ER:

**Table 5-2. Key Reactions Assumed to Occur in a Gasifier**

| <i>Rxn. #</i> | <i>Reaction Name</i>      | <i>Reaction</i>   |
|---------------|---------------------------|---|
| 1             | CO Oxidation              | $\text{CO(g)} + \frac{1}{2} \text{O}_2\text{(g)} \rightarrow \text{CO}_2\text{(g)}$                         |
| 2             | H <sub>2</sub> Oxidation  | $\text{H}_2\text{(g)} + \frac{1}{2} \text{O}_2\text{(g)} \rightarrow \text{H}_2\text{O(g)}$                 |
| 3             | CH <sub>4</sub> Oxidation | $\text{CH}_4\text{(g)} + \frac{1}{2} \text{O}_2\text{(g)} \rightarrow \text{CO(g)} + 2\text{H}_2\text{(g)}$ |

**Table 5-3. Key Tar Cracking and Oxidation Reactions Assumed to Occur in a Gasifier**

| <i>Rxn. #</i> | <i>Reaction</i>                                       |
|---------------|---|
| T1            | $C_6H_6(g) + 4.5O_2(g) \rightarrow 6CO(g) + 3H_2O(g)$ |

Figures 5-13, 5-14, and 5-15 show how the syngas composition (as predicted with M4) changes with increasing ER at constant temperatures of 1200 °F, 1300 °F, and 1400 °F. Figure 5-13 shows a slight decrease in CO<sub>2</sub> and a slight increase in CO which does not match with the literature. Figures 5-14 and 5-15 show trends matching literature data: CO<sub>2</sub> increases, and CO, C<sub>6</sub>H<sub>6</sub>, H<sub>2</sub> and CH<sub>4</sub> all decrease. Hence the concentrations of combustible gases in the syngas decrease because the excess air favors oxidation reactions in the gasifier (de Andrés, 2011). Figure 5-4 shows relatively equal decreases in H<sub>2</sub> and CO with increasing ER. This trend can also be seen in the experiment produced by Radmanesh et al. (2006). Figure 5-16 shows with increasing ER, the higher heating value (HHV) of the gas decreases (as expected with the decrease in combustible gases as mentioned above).

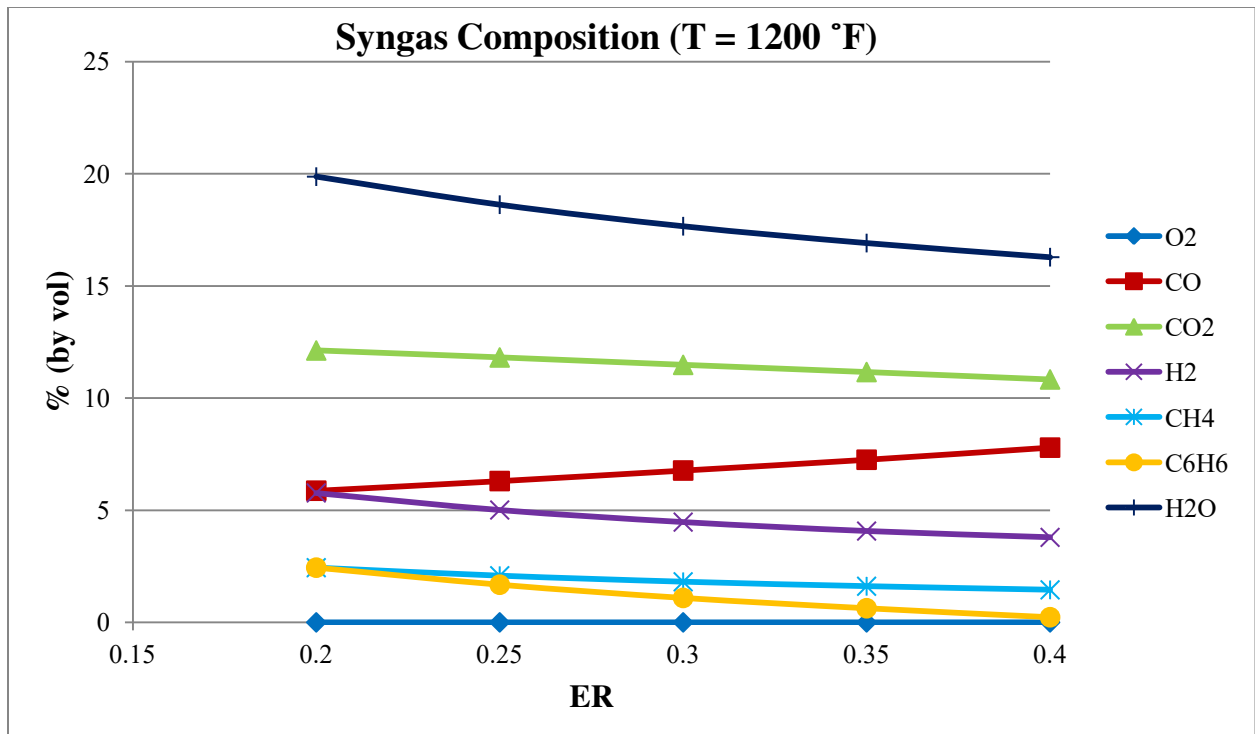


Figure 5-13. Syngas Composition vs Varying ER, T=1200 °F

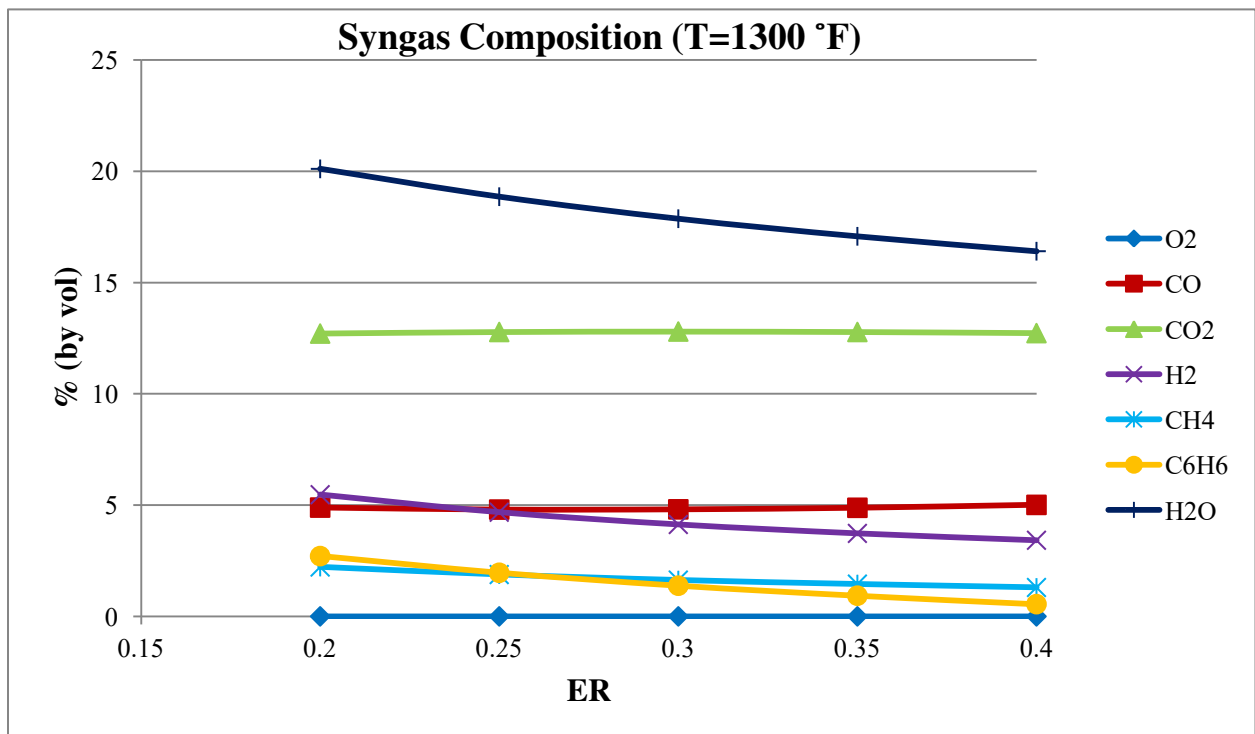


Figure 5-14. Syngas Composition vs Varying ER, T=1300 °F

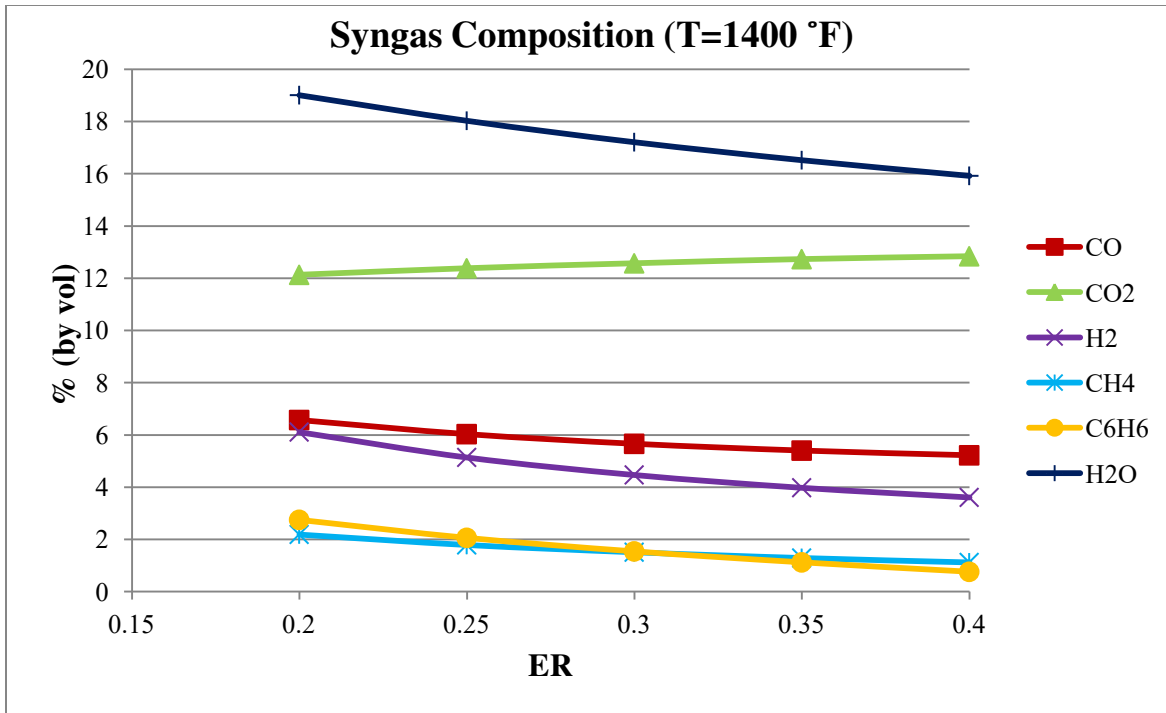


Figure 5-15. Syngas Composition vs Varying ER, T=1400 °F

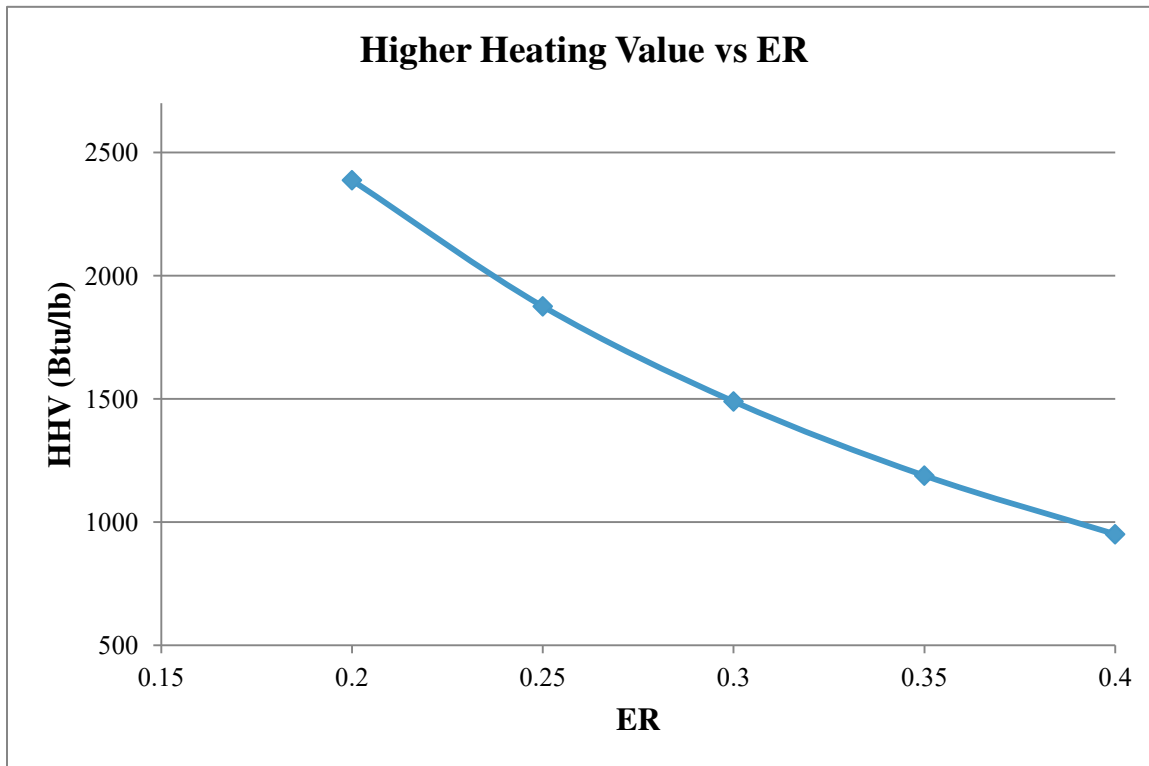


Figure 5-16. Higher Heating Value vs Varying ER, 1300°F

### 5.3.2 *Varying Temperature at Constant Equivalence Ratio*

Figures 5-17, 5-18, and 5-19 show the changes in syngas concentrations with changes in bed temperature (1200 °F to 1500 °F) at a constant ER. Changes in bed temperature affect all of the chemical reactions occurring in the gasifier. Increases in temperature promote the production of combustible gases CO and H<sub>2</sub> and hinder the production of CO<sub>2</sub> (Narváez et al., 1996; Radmanesh et al., 2006). Tar production also decreases with increasing bed temperatures due to the increase in tar cracking and steam reforming reactions (de Andrés et al., 2011; Manyà et al., 2006; Narváez et al., 1996). The M4 model results show these trends as discussed in the following paragraphs.

At higher ERs, CH<sub>4</sub> production and C<sub>6</sub>H<sub>6</sub> destruction slow with increasing temperatures. However, the most significant changes in the heating value of the gas (looking at the concentrations of CO, H<sub>2</sub>, and CH<sub>4</sub>) occur between 1380 °F and 1500 °F. This increase in heating value corresponds well with the increases shown in the literature (Radmanesh et al., 2006; Petersen & Werther, 2005).

A higher bed temperature produces a more valuable syngas but sewage sludge ash is prone to agglomeration and sintering at high temperatures, so temperatures above 1400 °F are not recommended for sewage sludge gasification (MaxWest Environmental Systems, Inc., 2013). It is also evident that even at higher temperatures, a higher ER has a negative effect on the concentration of combustible gases in the syngas. Experimental literature has shown that increases in temperature in sewage sludge gasifier-bed improve the heating value of the gas until the temperature reaches 1470 °F for a BFB gasifier and 1340 °F for a CFB gasifier (Kang et al., 2011; Petersen & Werther, 2005). However, at bed temperatures above 1400 °F, the model results still show an increase in heating value of the syngas.



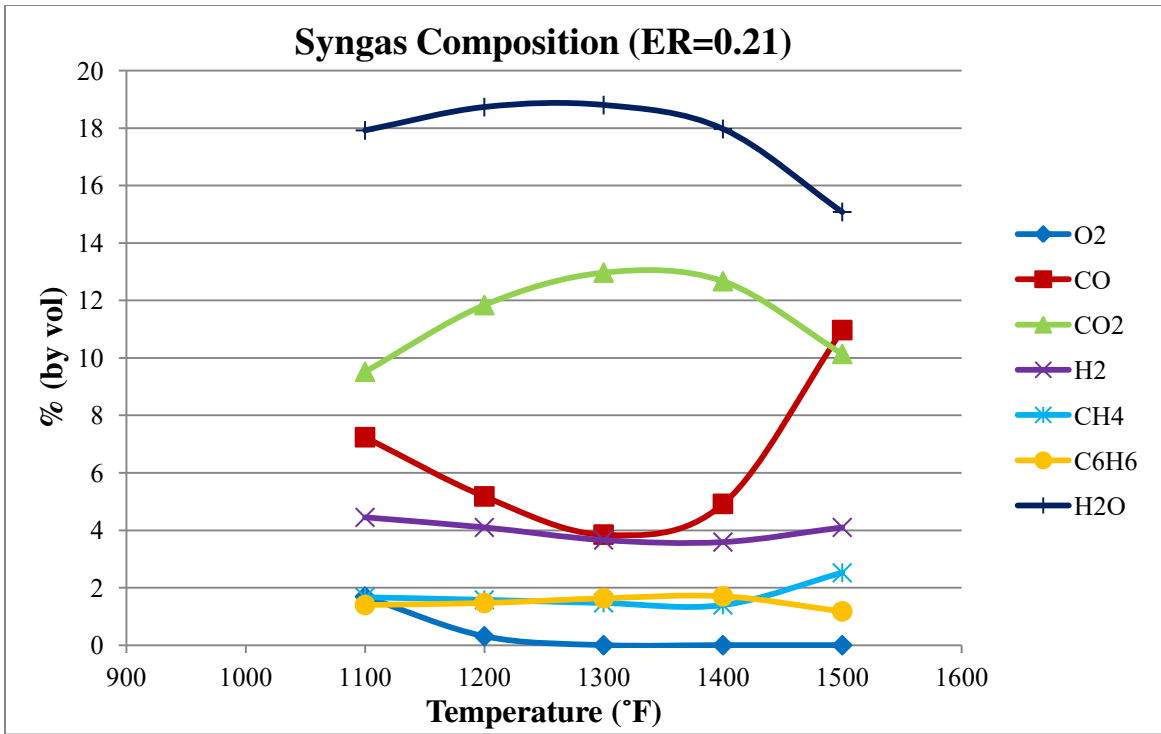


Figure 5-17. Syngas Composition vs Varying Temperature, ER=0.21

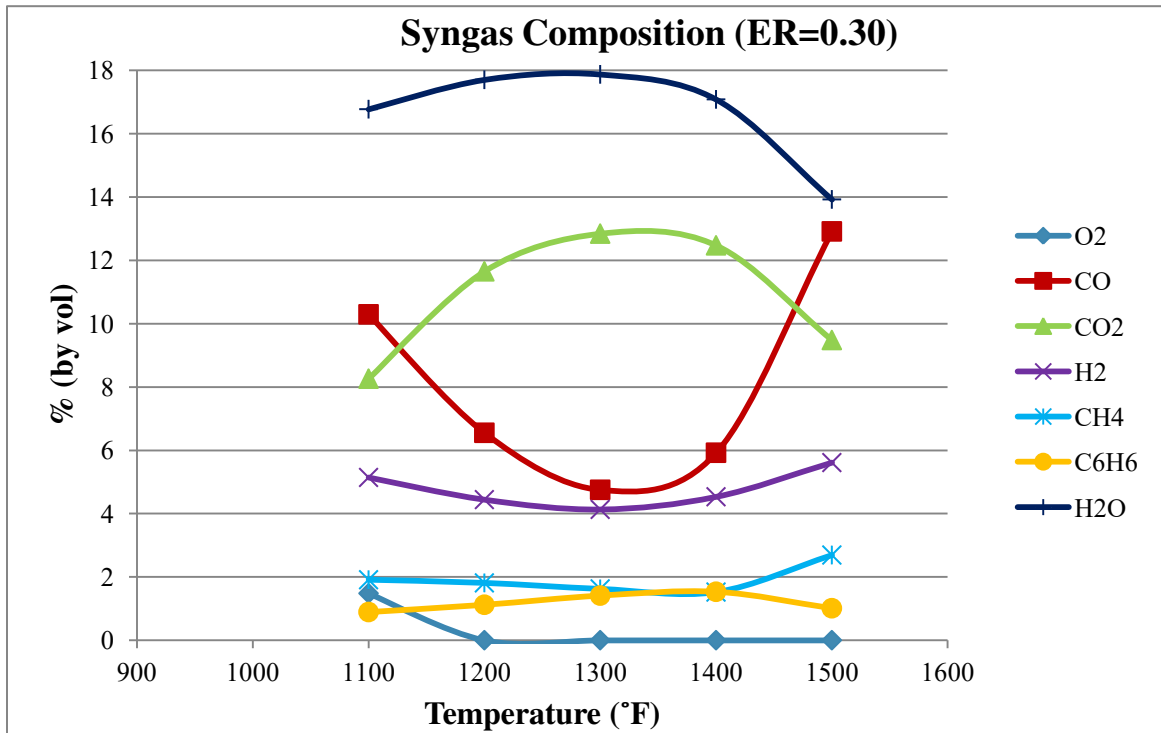
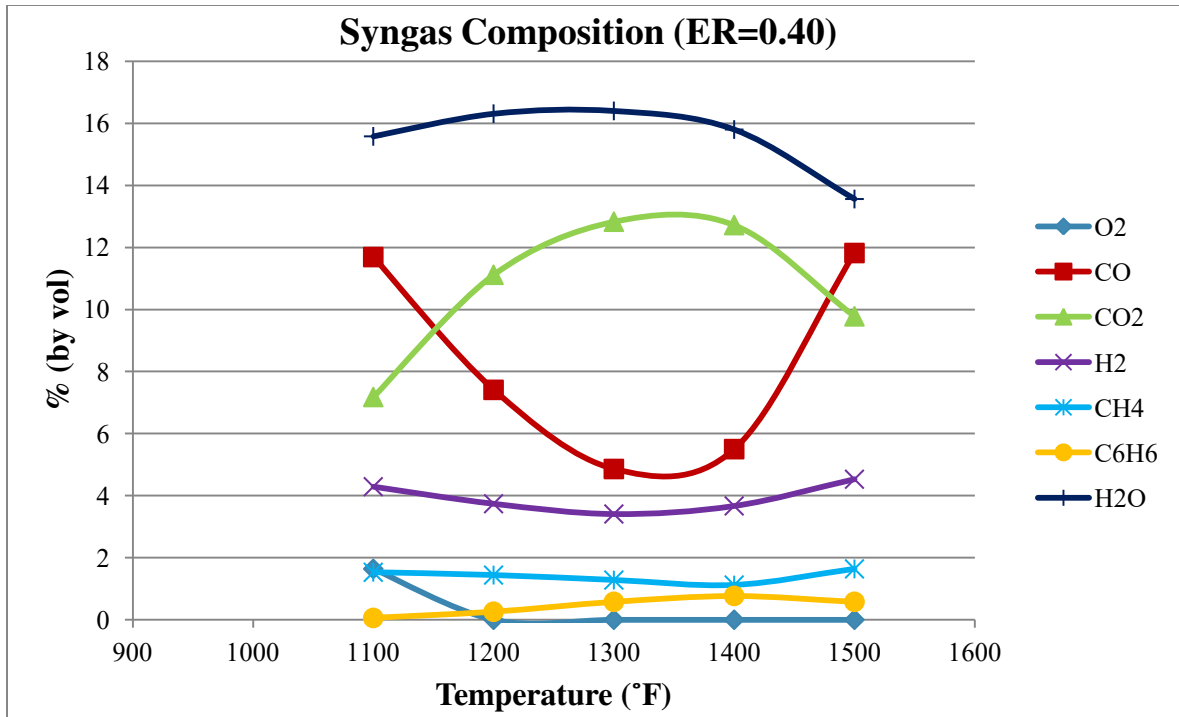


Figure 5-18. Syngas Composition vs Varying Temperature, ER=0.30



**Figure 5-19. Syngas Composition vs Varying Temperature, ER=0.40**

### 5.3.3 Varying Biosolid Composition

Although sludge composition is often an independent variable that ranges from location to location, an understanding of the effects of the biosolid composition on gasifier syngas can help in the design of the gasification facility in such ways as determining the amount of auxiliary fuel needed, and designing downstream APC.

For each of the following sections, the input composition (C, H, and N) of the biosolids used in the model was either increased or decreased while the remaining oxygen in the biosolids was increased or decreased accordingly.

### 5.3.3.1 Carbon

A 20% increase in fuel-C (oxygen ultimate analysis value was decreased accordingly) resulted in a 96% increase in tars whereas CO and CO<sub>2</sub> remained relatively stable and CH<sub>4</sub> decreased by 66%. These results slightly contradict the results mentioned by Champion et al. (2014) who saw an increase in CO, CO<sub>2</sub>, and tars by 12%, 17% and 39% respectively as well as a decrease in CH<sub>4</sub> by 51%, all with an increase of fuel-C of 20%.

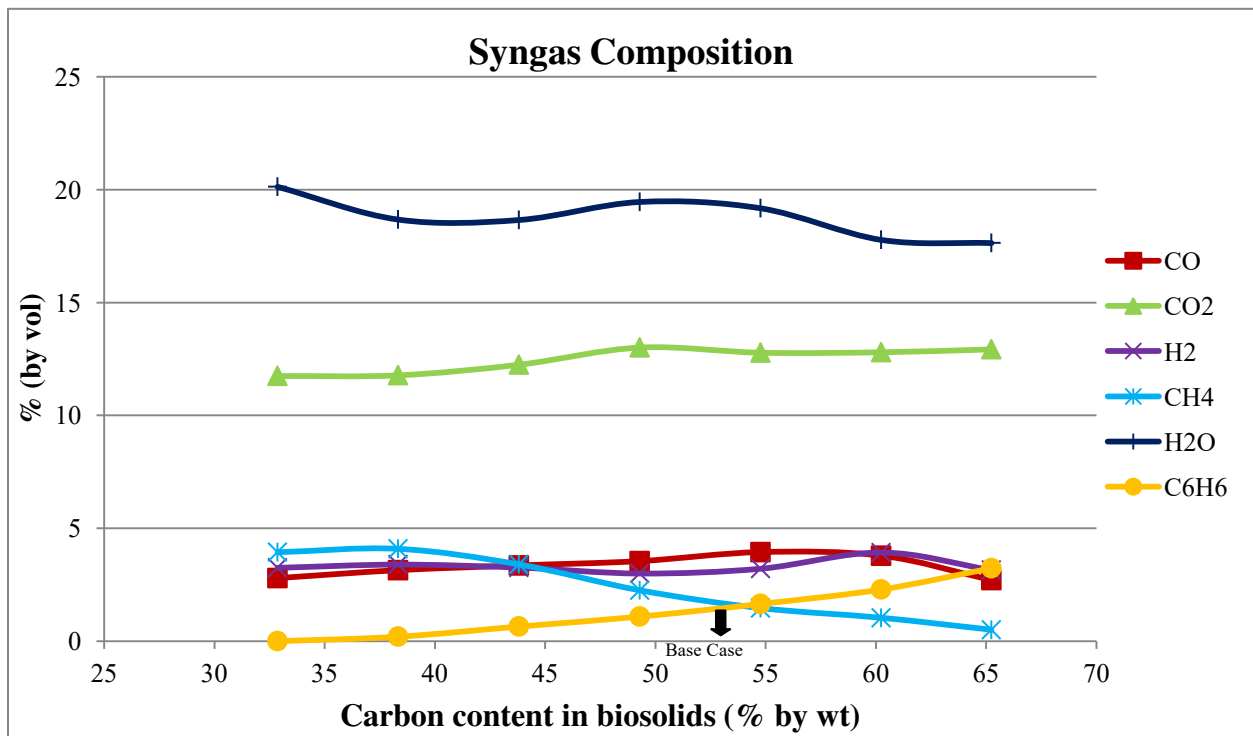
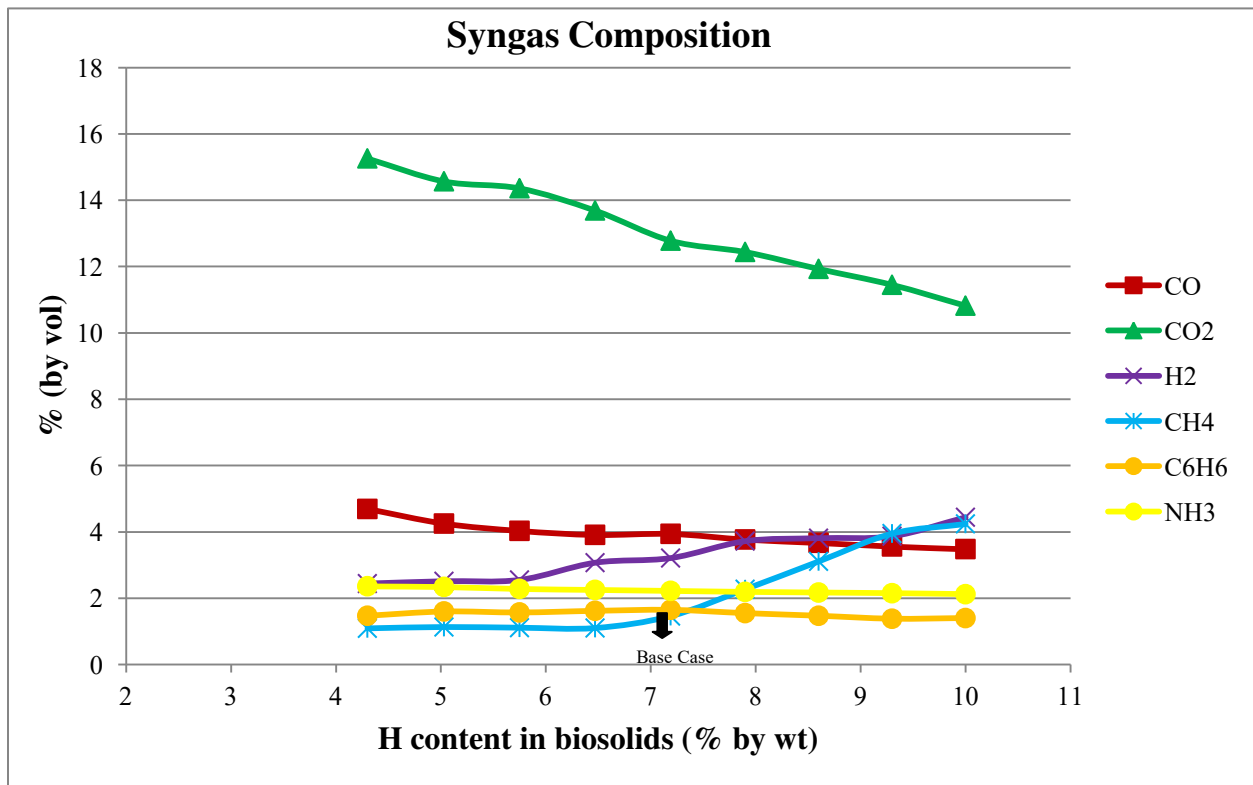


Figure 5-20. Syngas Composition vs Varying Carbon Content in Feed, ER=0.21, T=1300°F

### 5.3.3.2 Hydrogen

M4 is not as sensitive to changes in fuel-H (compared to M1) with the kinetic constant changes made to the Boudouard and water-gas shift reactions. A 20% decrease in fuel-H (and oxygen ultimate analysis value decreased accordingly) resulted in a 21% decrease in H<sub>2</sub>, and a 24% decrease in CH<sub>4</sub>. Carbon dioxide increased by 12% while the CO concentration remained stable. The results achieved by Champion et al. (2014) when the fuel-H was decreased by 20% was a decrease in H<sub>2</sub> by 18%, a decrease in CH<sub>4</sub> by 54%, and increases in CO and CO<sub>2</sub> concentrations by 5.3% and 17% respectively.



**Figure 5-21. Syngas Composition vs Varying Hydrogen Content in Feed, ER=0.21, T=1300°F**

### 5.3.3.3 Nitrogen

Figure 5-22 shows that by increasing the nitrogen content in the fuel, there is a corresponding increase in production of  $\text{NH}_3$  in the syngas. A 20% increase in fuel-N leads to a 20% increase in  $\text{NH}_3$  in the syngas. This trend between fuel-N and  $\text{NH}_3$  is a stoichiometric effect written into the model, not a kinetic effect. In the model it is assumed that 60% of fuel-N goes to  $\text{NH}_3$  and 40% goes to  $\text{N}_2$ . When gasifying a biomass that is fuel-N rich, it might be necessary to include downstream treatment to control  $\text{NO}_x$  after burning the syngas.

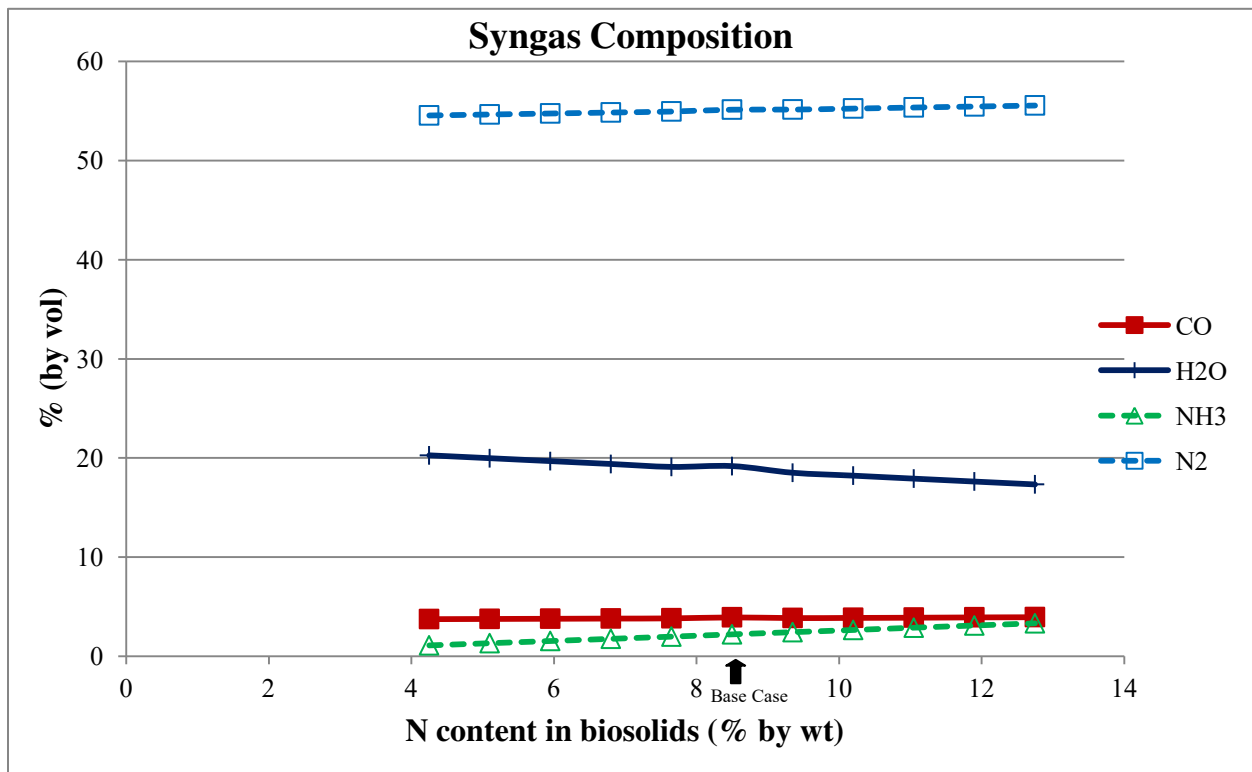


Figure 5-22. Syngas Composition vs Varying Nitrogen Content in Feed, ER=0.21, T=1300°F

## 6. RESULTS AND MODEL IMPROVEMENTS

### 6.1 Final Model

Several changes were made to the model based on using measurements of operational temperatures to determine a heat loss coefficient for the gasifier. After averaging the operational data of the gasifier collected over four months, it was discovered that the gasifier was being operated at a lower bed temperature than initially assumed. The minimum default input bed temperature was changed from 1160 °F (900 K) to 800 °F (700 K).

The as-built dimensions for the gasifier were made available after the initial version of the model was written, so the default input bed diameter and height were changed to the actual dimensions of 52.5 inches and 72 inches respectively. Using the correct bed dimensions allows for a more accurate model.

The initial density of the bed material (silica sand) was assumed to be  $1.50 \times 10^6 \text{ g/m}^3$ . After conducting the experiment detailed in Section 3.1.1, the actual density of the sand was found to be  $2.63 \times 10^6 \text{ g/m}^3$ . This change in density did not significantly affect the heat loss occurring throughout the gasifier bed.

Once a heat loss coefficient was determined for the gasifier (see Section 4.2), more code needed to be included in the model to calculate heat loss as a function of the heat loss coefficient, area of each zone, and the temperature difference between the temperature in the zone and the ambient temperature instead of simply assuming heat loss as a percentage. The method of calculating heat loss with a coefficient is a more accurate method than using an overall percentage. In each zone (A1-A5 and B1-B5) the equation below was included:

$$HL = UA\Delta T \quad (6-1)$$

Where:

HL = heat loss (J/s)

U = heat loss coefficient (J/m<sup>2</sup>-s-K)

A = heat transfer area of zone (m<sup>2</sup>)

$\Delta T = T_{\text{zone}} - T_{\text{ambient}}$  = difference in temperature between zone and ambient (K)

The heat loss coefficient (U) was then made into a user input parameter with the default equal to 4.0 J/m<sup>2</sup>-s-K. Changes were made to the GUI to accommodate input of the coefficient instead of the percentage (see Figure 6-1). The area of each zone was calculated by dividing the height of the gasifier bed (72 in) by the total number of zones (10) and then multiplying the diameter of the gasifier by pi and then by the zone height (7.2 in). The zone temperature ( $T_{\text{zone}}$ ) is calculated in the code for each zone based on the kinetic reactions taking place in that zone. The ambient temperature ( $T_{\text{ambient}}$ ) was assumed to be 85°F.

The averaged operational data previously presented in Tables 3-1 and 3-2 were used as default input values for the gasifier model (see Figure 6-1).


**Chemical Kinetic Model for a Fluidized-Bed Sewage Sludge Gasifier**  
Ver. 1.05 - July 2014

**Ultimate Analysis** Defaults  
Dry, ash-free

Carbon  % by wt.  
Hydrogen  % by wt.  
Oxygen  % by wt.  
Nitrogen  % by wt.  
Sulfur  % by wt.  
Chlorine  % by wt.  
Sum

**Proximate Analysis** Defaults  
As received

Moisture  % by wt.  
Organics  % by wt.  
Ash  % by wt.  
Sum



**Flue Gas Recirculation** Defaults

FG O2 %  % by vol.  
FG CO2 %  % by vol.  
FG H2O %  % by vol.  
FG N2 %  % by vol.  
Sum   
FGR Rate  lbs/hr  
FG Temp.  K

Developed at UCF  
PI: Dr. C. David Cooper  
Developer: Wyatt Champion  
Modified by: Hannah McLean

**Operations and Design** Defaults

Bed diameter  inches  
Bed height  inches  
Bio temp.  K  
Air temp.  K  
Sludge feed rate  lbs/hr  
Dry air rate  lbs/hr  
ER

Heat Loss U  J/(s-m2-K)  
Assumed Bottom Temp.  K  
 °F

Run Model

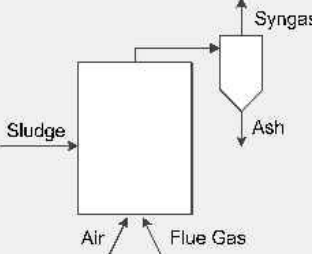


**Figure 6-1. Gasifier Model GUI-Inputs Screen**

Additional heat loss calculations were added to the model to account for heat loss through the freeboard of the gasifier. The final syngas temperature displayed on the Results GUI and the Model Output Excel spreadsheet is the temperature of the syngas exiting the top of the gasifier (see Figures 6-2 and 6-3); the final syngas temperature previously was the temperature of the syngas exiting the fluidized bed in the gasifier. This addition to the model provided a final syngas temperature that is very close to the final syngas temperature obtained from operational data (see Figure 4-4). The final syngas composition in Figures 6-2 and 6-3 is derived from the default input values.



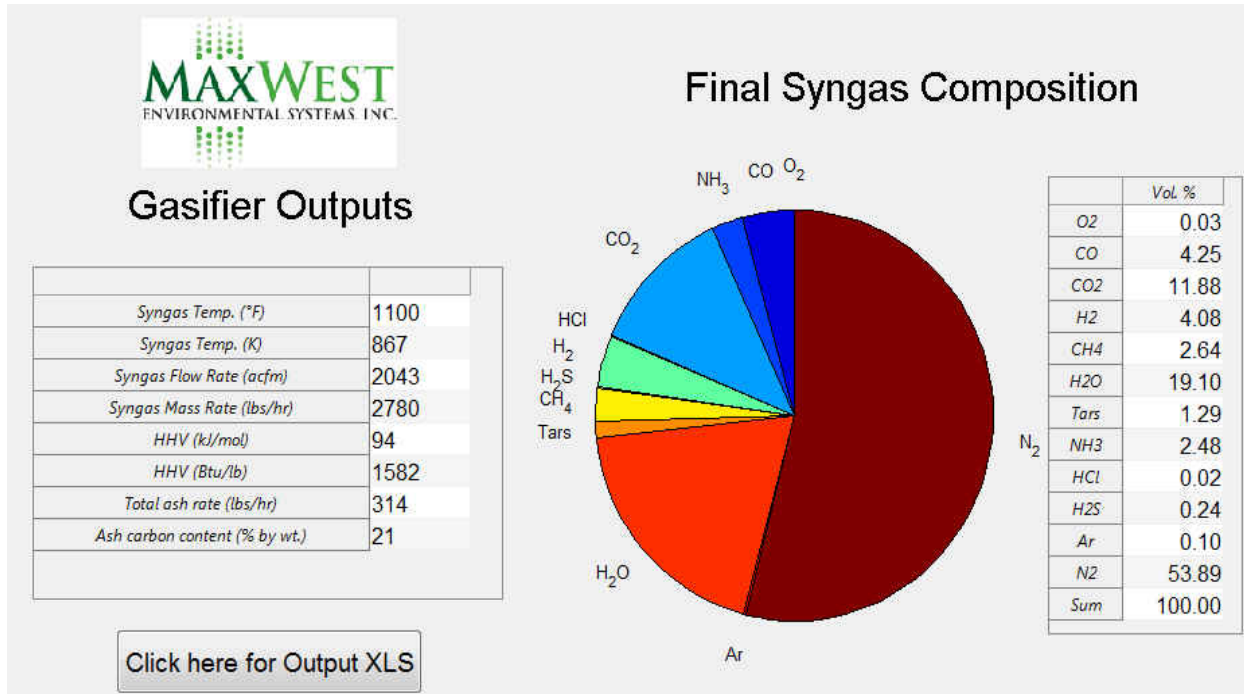


Figure 6-2. Gasifier Model GUI-Outputs Screen

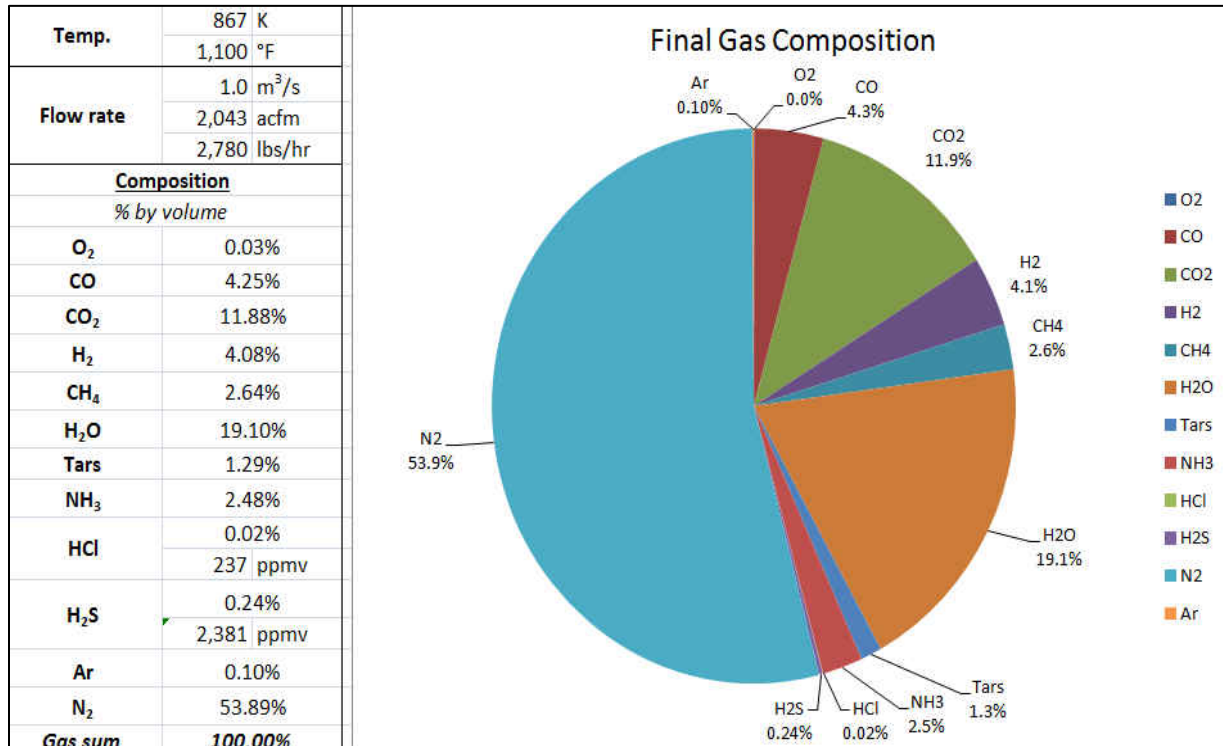


Figure 6-3. Base Case Results

Changes were made to the kinetic constants of two of the reactions in the model, namely the pre-exponential factors for the Boudouard and water-gas shift reactions. The decision to change these kinetics resulted from the sensitivity analyses conducted on the model to see how the syngas composition changed with changes in ER and temperature. It was observed that with increasing bed temperature (at a constant ER), the concentration of CO was decreasing and the concentration of CO<sub>2</sub> was increasing. These findings contradicted the results reported in the literature (de Andrés et al., 2011; Narváez et al., 1996; Petersen & Werther, 2005; Kang et al., 2011; Radmanesh et al., 2006).

The original pre-exponential constants for the Boudouard and water-gas shift reactions were  $3.18 \times 10^5$  and  $2.78 \times 10^{-2}$  respectively (Champion et al., 2014). To correct these trends, the decision was made to change the pre-exponential terms for the water-gas shift and Boudouard reactions back to the original literature values (see Equations 5-2 and 5-4) (Petersen & Werther, 2005). These changes caused the trends in syngas composition changes with increasing temperatures to more closely match literature trends. Figure 5-16 shows that with increasing bed temperature, the concentration of CO increases, CO<sub>2</sub> decreases, H<sub>2</sub> increases, and C<sub>6</sub>H<sub>6</sub> decreases.

Although it appears in Figures 5-5 and 5-7 that M4 is not predicting the exit syngas composition as well as M1, this is only in the limited range of three experimental studies. It is still recommended to keep the reaction rates suggested in this work because the overall predicted syngas trends match the literature trends over a wider range of temperature and ER (de Andrés et al., 2011; Narváez et al., 1996; Kang et al., 2011; Petersen & Werther, 2005; Radmanesh et al., 2006). Champion et al. (2014), changed the reaction rates arbitrarily to achieve a better “goodness-of-fit” (see Figures 5-4, 5-6, 5-8, and 5-10).

Biosolids gasification provides a usable, energy rich syngas and reduces the dependency on fossil fuels. The modified model provides a prediction of the syngas produced and allows for the further refinement of input parameters by facility operators.

## 7. CONCLUSIONS AND RECOMMENDATIONS

### 7.1 Utility of the Model

The use of chemical kinetics is important in developing a robust and accurate model to predict the syngas rate and composition from a fluidized-bed biomass gasifier. A few literature studies report on experiments conducted on gasifiers, and others report on models used to predict gasifier syngas composition, however many of the parameters developed for the models were obtained from gasification of coal or woody biomass and the experiments were conducted at a laboratory scale. In the development of a sewage sludge gasification model, modifications to previously reported reaction kinetics as well as the assumptions for the splitting of initial devolatilization products may be necessary.

A model that produces results, which compare well with literature values, can be a very useful tool for gasification facilities. An effective model must accurately account for heat loss throughout the gasifier so that the syngas predictions and designs of downstream equipment will be accurate. Commercial-scale gasification facilities control bed temperature by increasing or decreasing the air-to-fuel ratio (equivalence ratio) entering the gasifier, therefore a useful model should include this parameter as an input so the operators can see how changing the ratio will affect the output syngas composition.

A robust and accurate gasification model may aid in the design and improvement of downstream APC devices as well as the more efficient use of auxiliary fuel. The effects of varying feedstock on the performance of a gasifier are important to gasification facility operators. By estimating the energy content of a syngas before it is produced, operators can

reduce the need for extra fuel and can better understand which fuels produce more energy or which produce more tars that they will then have to control downstream.

## 7.2 Recommendations for Future Research

The main recommendation to further improve a biosolids gasifier model would be to sample and analyze the biosolids (fuel), ash, air inputs, and syngas produced from the operating gasifier during steady-state. This is a difficult and expensive undertaking due to the temperature and ignitability of the syngas as well as the cost of collecting, transporting, and analyzing the samples. These are the reasons why this task was not performed in this author's scope of work. However, such analyses would give necessary data that would make the model predictions more robust and would aid in the design and operation of other commercial-scale gasification facilities. It is recommended that the data collections be conducted over wider temperature and ER ranges.

It is recommended that more studies focus on the initial stages of gasification especially with regard to the fate of the nitrogen in the biosolids. The model (M4) assumes that 60% of fuel-N goes to  $\text{NH}_3$  and 40% goes to  $\text{N}_2$  which greatly influences  $\text{NO}_x$  formation in the thermal oxidizer. Future research should analyze how the fuel-N is split between  $\text{N}_2$  and  $\text{NH}_3$  in the gasifier.

**APPENDIX:  
SUGGESTIONS FOR RUNNING THE GASIFICATION MODEL**

- Try to refrain from resizing the input screen when running. This will slow down the program.
- If trying to close the input screen while running the program, click the “X” button in the upper right hand corner of the black command window. This will close the Gasifier GUI.
- To view the model output spreadsheet, click on “Click here for Output XLS” button on the Results GUI. This will open the model output spreadsheet. Click on the “Model Output” tab to view the syngas composition throughout the gasifier as well as the final syngas data that is shown on the Results GUI.

## REFERENCES

- Adegoroye, A., Paterson N., Li, X., Morgan, T., Herod, A., Dugwell, D. et al. (2004). The characterisation of tars produced during the gasification of sewage sludge in a spouted bed reactor. *Fuel*, 83, 1949-1960. doi:10.1016/j.fuel.2004.04.006.
- Auxilio, A., Dayal, S., Chen, L., Kirtania, K., & Bhattacharya, S. (2011). Disposal of Biosolids: A Study Using Thermogravimetric Analysis. *Chemeca*, 1789-1801.
- Basu, P. & Kaushal, P. (2009). Modeling of Pyrolysis and Gasification of Biomass in Fluidized Beds: A Review. *Chemical Product and Process Modeling*, 4, 1-45. doi:10.2202/1934-2659.1338.
- Basu, P., Acharya, B., & Dutta, A. (2010). Gasification in Fluidized Beds-Present Status & Design. *Proceedings of the 20<sup>th</sup> International Conference on Fluidized Bed Combustion*, 97-103.
- Cartmell, E., Gostelow, P., Riddell-Black, D., Simms, N., Oakey, J., Morris, J. et al. (2006). Biosolids-A Fuel or a Waste? An Integrated Appraisal of Five Co-combustion Scenarios with Policy Analysis. *Environmental Science Technology*, 40, 649-658. doi: 10.1021/es052181g.
- Champion, W.M., Cooper, C., Mackie, K., & Cairney, P. (2014). Development of a Chemical Kinetic Model for a Biosolids Fluidized-Bed Gasifier and the Effects of Operating Parameters on Syngas Quality. *Journal of the Air & Waste Management Association*, 64,160-174.
- de Andrés, J., Narros, A., & Rodríguez, M.(2011). Air-steam gasification of sewage sludge in a bubbling bed reactor: Effect of alumina as a primary catalyst. *Fuel Processing Technology*, 92, 433-440.doi:10.1016/j.fuproc.2010.10.006.



- Densities of Miscellaneous Solids. (n.d.). In *Engineering Toolbox online*. Retrieved from [http://www.engineeringtoolbox.com/density-solids-d\\_1265.html](http://www.engineeringtoolbox.com/density-solids-d_1265.html).
- Gómez-Barea, A. & Leckner, B. (2010). Modeling of biomass gasification in fluidized bed. *Progress in Energy and Combustion Science*, 36, 444-509. doi: 10.1016/j.peccs.2009.12.002.
- Gómez-Barea, A., Leckner, B., Perales, A., Nilsson, S., & Cano, D. (2013). Improving the performance of fluidized bed biomass/waste gasifiers for distributed electricity: A new three-stage gasification system. *Applied Thermal Energy*, 50, 1453-1462. doi: 10.1016/j.applthermaleng.2011.12.025.
- Houdková, L., Boran, J., Ucekaj, V., Elsasser, T., & Stehlik, P. (2008). Thermal processing of sewage sludge-II. *Applied Thermal Engineering*, 28, 2083-2088. doi: 10.1016/j.applthermaleng.2008.04.005.
- Kang, S., Dong, J., Kim, J., Lee, W., & Hwang, W. (2011). Gasification and its emission characteristics for dried sewage sludge utilizing a fluidized bed gasifier. *Journal of Material Cycles Waste Management*, 13, 180-185. doi:10.1007/s10163-011-0016-y.
- Kaushal, P., Proll, T., & Hofbauer, H. (2007). Model Development and validation: Co-combustion of residual char, gases and volatile fuels in the fast fluidized combustion chamber of a dual fluidized bed biomass gasifier. *Fuel*, 86, 2687-2695. doi: 10.1016/j.fuel.2007.03.032.
- Liu, H., & Gibbs, B. (2002). Modeling NH<sub>3</sub> and HCN emissions from biomass circulating fluidized bed gasifiers. *Fuel*, 82, 1591-1604. doi:10.1016/S0016-2361(03)00091-7.
- Manyà, J.J., Aznar, M., Sánchez, J.L., Arauzo, J., & Murilla, M.B. (2006). Further Experiments on Sewage Sludge Air Gasification: Influence of the Nonstationary

- Period on the Overall Results. *Industrial & Engineering Chemistry*, 45, 7313-7320.  
doi:10.1021/ie0605027
- Maxwest Environmental Systems, Inc. (2012). Report from Experiments Performed with a  
Lab-scale Fluidized-bed Sewage Sludge Gasifier.
- MaxWest Environmental Systems, Inc. (2012). *Technical Data Sheet Model: MW 2000*.  
Sanford, FL: Author.
- Mendenhall, W., and T. Sincich. (2007). *Statistics: For Engineering and the Sciences*. Upper  
Saddle River, NJ: Pearson Prentice Hall.
- Miao, Qi. (2010). Doctoral Dissertation: Modeling Biomass Gasification in Circulating  
Fluidized Beds. The University of Western. Ontario, Canada.
- Miao, A., Zhu, J., Barghi, S., Wu, C., Yin, X., & Zhou, Z. (2014). Model validation of a CFB  
biomass gasification model. *Renewable Energy*, 63, 317-323. doi:  
10.1016/j.renene.2013.09.040.
- Narváez, I., Orío, A., Aznar, M.P. & Corella, J. (1996). Biomass Gasification with Air in an  
Atmospheric Bubbling Fluidized Bed. Effect of Six Operational Variables on the  
Quality of the Produced Raw Gas. *Industrial and Engineering Chemistry Research*,  
35, 2110-2120. doi:10.1021/ie9507540.
- Petersen, I., & Werther, J. (2005). Experimental Investigation and modeling of gasification of  
sewage sludge in the circulating fluidized bed. *Chemical Engineering and  
Processing*, 44, 717-736. doi:10.1016/j.cep.2004.09.001.
- Puig-Arnabat, M., Bruno, J.C., & Coronas, A. (2010). Review and analysis of biomass  
gasification models. *Renewable and Sustainable Energy Reviews*, 14, 2841-2851. doi:  
10.1016/j.rser.2010.07.030.

- Radmanesh, R., Chaouki, J., & Guy, C. (2006). Biomass Gasification in a Bubbling Fluidized Reactor: Experiments and Modeling. *American Institute of Chemical Engineers Journal*, 52, 4258-4272. doi:10.1002/aic.11020.
- Roy, M., Dutta, A., Corscadden, K., Havard, P., & Dickie, L. (2011). Review of biosolids management options and co-incineration of a biosolid-derived fuel. *Waste Management*, 31, 2228-2235. doi: 10.1016/j.wasman.2011.06.008.
- Santoleri, J.J., Reynolds, J., & Theodore, L. (2000). *Introduction to Hazardous Waste Incineration*. New York: Wiley-Interscience. pp.175-182.
- Sharma, A. (2008). Equilibrium modeling of global reduction reactions for a downdraft (biomass) gasifier. *Energy Conversion and Management*, 49, 832-842. doi: 10.1016/j.enconman.2007.06.025.
- Slade, R. (2010). *Specific Gravity of Soils Determination*. Orlando, FL: University of Central Florida.
- University of Hawaii, Hawaii Natural Energy Institute. (2002). Analysis of Hawaii Biomass Energy Resources for Distributed Energy Applications.
- Wang, F., Rudolph, V., & Zhu, Z. (2008). Sewage Sludge Technologies. *Ecological Engineering*, 3227-3242. doi: 10.1016/B978-008045405-4.00078-1.
- Werther, J., & Ogada, T. (1999). Sewage sludge combustion. *Progress in Energy and Combustion Science*, 25, 55-116. doi: 10.1016/S0360-1285(98)00020-3.
- Yan, H., Heidenreich, C., & Zhang, D. (1999). Modelling of bubbling fluidized bed coal gasifiers. *Fuel*, 78, 1027-1047. doi: 10.1016/S0016-2361(99)00028-9.

Yuan, X., Huang, H., Zeng, G., Li, H., Wang, J., Zhou, C., et al. (2011). Total concentrations and chemical speciation of heavy metals in liquefaction residues of sewage sludge.

*Bioresource Technology*, 102, 4104-4110. doi: 10.1016/j.biortech.2010.12.055.